

Structural Properties and Degree of Intramolecular Charge Transfer of an *N*-Alkyl Indoline–Tricyanoquinodimethane System

Tsuyoshi Murata,*[1] Kazukuni Nishimura,[1] Yuichiro Enomoto,[1] Genki Honda,[1] Yasuhito Shimizu,[1] Akihiro Otsuka,[2] and Gunzi Saito*[1,2]

[1]Division of Chemistry, Graduate School of Science, Kyoto University, Sakyo-ku, Kyoto 606-8502

[2]Research Center for Low Temperature and Materials Sciences, Kyoto University, Sakyo-ku, Kyoto 606-8502

Received January 7, 2008; E-mail: saito@kuchem.kyoto-u.ac.jp

A series of intramolecular charge-transfer compounds comprised of 1-alkyl-3,3-dimethyl-2-methyleneindoline (**I**$_n$, donor, n = alkyl chain length; 1–8, 10, 14, 16, 18, 20, and 22) and 7,8,8-tricyanoquinodimethane (=2-(4′-cyanomethylene-2′,5′-cyclohexadienylidene)malononitrile (3CNQ), acceptor) moieties linked through a π-bond, **I**$_n$–3CNQ were prepared, and their structures are discussed. The melting points of the **I**$_n$–3CNQ solids decreased with increasing alkyl chain length until reaching a minimum point (95 °C) at $n = 18$, and then began to gradually increase, indicating self-aggregation of the alkyl chains. The **I**$_n$–3CNQ derivatives with long alkyl chains ($n \geq 6$) produced supercooled liquids displaying conspicuous color changes after melting. Diverse molecular packing patterns were observed in the crystal structures. Most **I**$_n$–3CNQ derivatives formed face-to-face and/or side-by-side dimeric motifs to cancel net dipole moments. **I**$_{20}$–3CNQ formed a two-dimensional bilayer structure by π-stacking and self-assembly of the alkyl chains. Two types of molecular conformation, which significantly affect the electronic structures, were observed to be dependent on the alkyl chain length. A parameter to evaluate the degree of intramolecular charge transfer, namely bond length ratio, was proposed; it exhibited good agreement with solvatochromic shifts and molecular orbital calculations.

Intramolecular charge-transfer (CT) compounds $D^{\delta+}$–π–$A^{\delta-}$ (δ = degree of CT), comprised of donor (D) and acceptor (A) moieties linked by a π-bond, have been intensively studied for the development of various functional organic materials, such as unimolecular rectifiers[1–4] and non-linear optical materials,[5–9] by taking advantages of their flexible electronic structure, redox ability, and large dipole moments. In particular, products of the Stork enamine reaction between tertiary amine derivatives (*N*-alkyl picolinium, lepidinium, benzothiazolium, etc.) and strong electron acceptors (7,7,8,8-tetracyanoquinodimethane (TCNQ),[1–7,10–12] tetracyanoethylene (TCNE),[8,9,13] and *p*-chloranil[14]) have attracted considerable attention with respect to the molecular and solid-state properties of $D^{\delta+}$–π–$A^{\delta-}$ solids. The degree of CT (δ), which indicates the charge distribution of a $D^{\delta+}$–π–$A^{\delta-}$ molecule, is one of the most important parameters when investigating their functionality; however, distinct methodologies to determine the δ values experimentally and quantitatively have not been proposed.[2,15,16] We have studied a series of $D^{\delta+}$–π–$A^{\delta-}$ compounds, indoline–tricyanoquinodimethane (=2-(4′-cyanomethylene-2′,5′-cyclohexadienylidene)malononitrile) derivatives (Chart 1, **I**$_n$–3CNQ-R ($n = 1$), where n and R represent the number of carbon atoms in an alkyl group attached to the indoline N atom and a substituent group attached to the 3CNQ moiety, respectively) derived from the Stork enamine reaction between 1,3,3-trimethyl-2-methyleneindoline and R-TCNQ (Chart 1).[17,18] In the previous paper, we successfully established a methodology to estimate the δ values of the molecules in the solution state by taking advantage of their solvatochromic behavior and revealed that the δ values of **I**$_n$–3CNQ-R varied with the strength of the electron-withdrawing ability of substituents on the 3CNQ moiety (R).[18]

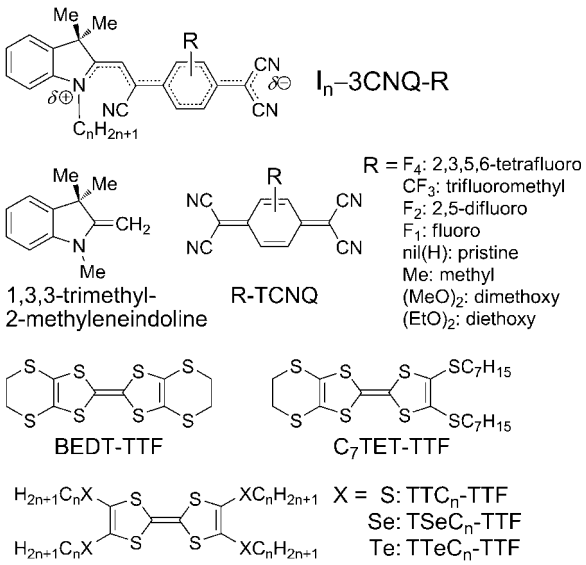

Chart 1. Chemicals discussed in the text.

Long alkyl chain groups aggregate in the solid state and can control molecular packing (Fastener effect).[19] In tetra(alkylchalcogeno)-substituted tetrathiafulvalene (=2-(1′,3′-dithiol-2′-ylidene)-1,3-dithiole, TTF) derivates (TXC$_n$-TTF, Chart 1), such self-aggregation ability of long alkyl chains tightly fastened the TTF π-moieties to form a conduction column and demonstrated a highly conductive solid of single-component

Published on the web July 10, 2008; doi:10.1246/bcsj.81.869

electron-donors.[19] $D^{\delta+}$–π–$A^{\delta-}$ molecules having long alkyl or thioacetylalkyl groups form Langmuir–Blodgett (LB) films[1] and self-assembled monolayers,[5] and unimolecular electrical rectification has been observed in these films.[1–4] Hybrid LB films composed of $\mathbf{I}_1$–3CNQ-R compounds (R = pristine and $(MeO)_2$) and clay have also been studied for second harmonic generation.[20] Determination of the molecular structure, crystal packing, and δ value is essential to explain the microscopic electronic structure of the solids and films for the research of functional materials based on $D^{\delta+}$–π–$A^{\delta-}$ type unimolecular organic molecules; however, structural analyses of $D^{\delta+}$–π–$A^{\delta-}$ molecules with long alkyl groups have rarely been reported.[10b]

In this study, we prepared a series of $\mathbf{I}_n$–3CNQ derivatives with a wide range of alkyl chain lengths (n = 1–8, 10, 14, 16, 18, 20, and 22, R = H) and investigated their thermal, redox, optical, and structural properties. To elucidate the functionalities of $D^{\delta+}$–π–$A^{\delta-}$ compounds, a comprehensive discussion of not only the electronic structure of a single molecule but also the molecular arrangement in the solid state is crucial. In this context, we discuss (1) the crystal packing of $\mathbf{I}_n$–3CNQ derivatives with respect to the cooperation between dipole–dipole and/or face-to-face interactions of the D–π–A skeletons and self-aggregation of the long alkyl chains, and (2) the estimation of δ values of $\mathbf{I}_n$–3CNQ-R molecules in the solid state. As for the estimation of δ values, we utilized the intramolecular bond lengths in crystal structure analysis and compared the estimated δ values to those evaluated from molecular orbital calculations. The effect of molecular conformations on these values is also discussed.

Experimental

Measurements and Calculations. ^{1}H NMR spectra were measured at 400 MHz on a JEOL JNM-FX400 spectrometer using $CDCl_3$ or DMSO-d_6 as a solvent and tetramethylsilane as an internal standard. Elemental analyses were performed at the Center for Organic Elemental Microanalysis, Kyoto University. Crystallization, melting, and decomposition temperatures were measured using differential scanning calorimetry (DSC) thermograms (1 or 10 K min^{-1} cooling/heating rate) on a Shimadzu-60 instrument, equipped with nitrogen cryostatic cooling. Cyclic voltammetry was measured in acetonitrile (MeCN) containing 0.1 M (1 M = 1 mol dm^{-3}) of n-$Bu_4N^+BF_4^-$ with Pt electrodes vs. SCE (saturated calomel electrode) at a scan rate of 50 mV s^{-1} using an ALS/chi Electrochemical Analyzer model 650A, operated at room temperature. Ultraviolet–visible (UV–vis) spectra were measured on a Shimadzu UV-3100 spectrometer in dry solvents (chlorobenzene (PhCl), acetone, MeCN, and methanol (MeOH)), KBr pellets, or on quartz plates. Infrared (IR) spectra were measured using a Perkin-Elmer Paragon 1000 in KBr pellets or on quartz plates (resolution of 2 or 4 cm^{-1}). Semi-empirical molecular orbital calculations were performed using MOS/F V4 with INDO/S parameterization coupled with a 20 dimension CI matrix, which are sufficient to give approximately invariant dipole moments. Geometrical parameters were extracted from the crystal structures.

Preparation of $\mathbf{I}_n$–3CNQs. $\mathbf{I}_n$–3CNQ derivatives were prepared by methods used for 3CNQ-type $D^{\delta+}$–π–$A^{\delta-}$ systems.[1,10b,11] 2,3,3-Trimethyl-3*H*-indole (**I**) and alkylhalide ($C_nH_{2n+1}X$, X = Br or I) were reacted to produce 1-alkyl-2,3,3-trimethyl-3*H*-indolium halide **II**. Salt **II** was neutralized with piperidine, and then in situ generated indoline **III** reacted with TCNQ under reflux giving $\mathbf{I}_n$–3CNQ (Scheme 1, Method 1). The reaction using isolated **III**, which was purified by extraction after neutralization, also gave $\mathbf{I}_n$–3CNQ (Scheme 1, Method 2). Solvents were dried and distilled under of nitrogen prior to use, and the reactions were performed in a nitrogen atmosphere. The appearance, melting point, and optical properties of $\mathbf{I}_n$–3CNQ derivatives are summarized in Table 1.

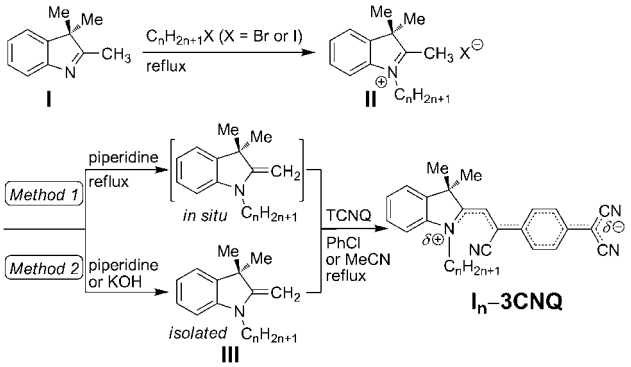

Scheme 1. Synthetic procedures for $\mathbf{I}_n$–3CNQ.

Typical Procedures for the Preparation. Method 1: Preparation of $\mathbf{I}_4$–3CNQ: 2,3,3-Trimethyl-3*H*-indole (**I**) (3.18 mL, 20.0 mmol) and 1-iodobutane (2.3 mL, 20 mmol) were refluxed in ethyl acetate (10 mL) for 20 h. After cooling, ether (70 mL) was added to the reaction mixture and stirred; the ether layer thus formed was removed by decantation. The oily residue was washed with a mixture of ethyl acetate and ether. The product was dried under reduced pressure to give 1-butyl-2,3,3-trimethyl-3*H*-indolium iodide (**II**) (3.18 g, 47%) in the form of a soft red powder. Salt **II** was used for the next reaction without further purification. Salt **II** (1.76 g, 5.13 mmol) was dissolved in PhCl (50 mL), piperidine (0.52 mL, 5.26 mmol) was then added to the solution. To this **III** solution, TCNQ (1.09 g, 5.34 mmol) dissolved in PhCl (80 mL) was added, and the mixture was refluxed for 1 h. After evaporation of the solvent, the crude product was purified by column chromatography ($CHCl_3$/ethyl acetate = 4:1, silica gel) and then recrystallized from MeCN to give green platelet crystals of $\mathbf{I}_4$–3CNQ (**4**) (304 mg, 15%).

Method 2: Preparation of $\mathbf{I}_5$–3CNQ: 1-Pentyl-2,3,3-trimethyl-3*H*-indolium iodide salt **II** was prepared by the same procedure as Method 1 (31% yield). Salt **II** (1.80 g, 5.03 mmol) was added to a KOH aqueous solution (85%, 20 mL), and the mixture was stirred for 1.5 h. The yellow oily product was extracted with ether (20 mL), and the organic extract was washed with a saturated NaCl aqueous solution (20 mL × 3), and then dried over $MgSO_4$ and concentrated under reduced pressure, to give neutral **III** (89%). TCNQ (912 mg, 4.47 mmol) dissolved in PhCl (70 mL) and crude **III** (1.00 g, 4.37 mmol) dissolved in PhCl (10 mL) were refluxed for 7 h. After evaporation of the solvent, the crude product was extracted with $CHCl_3$, the solvent was then removed by evaporation under reduced pressure. Green platelet crystals of $\mathbf{I}_5$–3CNQ (**5**) (700 mg, 39%) were obtained by recrystallization from MeCN (100 mL).

X-ray Crystal Structure Analyses. The crystal structures of $\mathbf{I}_n$–3CNQ derivatives, $\mathbf{I}_2$–3CNQ (**2**), ($\mathbf{I}_3$–3CNQ)(MeCN) (**3a**), ($\mathbf{I}_3$–3CNQ)$(C_6H_6)_{0.5}$ (**3b**), $\mathbf{I}_4$–3CNQ (**4**), $\mathbf{I}_5$–3CNQ (**5**), $\mathbf{I}_6$–3CNQ (**6a** and **6b**), ($\mathbf{I}_6$–3CNQ)(MeCN) (**6c**), $\mathbf{I}_7$–3CNQ (**7a** and **7b**), ($\mathbf{I}_8$–3CNQ)$(C_6H_6)_{0.5}$ (**8**), $\mathbf{I}_{10}$–3CNQ (**10**), and $\mathbf{I}_{20}$–3CNQ (**20**), were determined. The intensity data of the structural analy-

Table 1. Appearance, Melting Points, and UV–Vis Spectra of $\mathbf{I}_n$–3CNQ

Compound[a]		Color and shape of solid	Mp/°C[b]	UV–vis/nm[e] Solid (in KBr)	MeOH	MeCN	Acetone	PhCl	δ_{solv}
$\mathbf{I}_1$–3CNQ	**1**	green powder	233.0 (dec)[c]	858sh, 708	779, 720	787, 725	792, 726	794, 726	0.51
$\mathbf{I}_2$–3CNQ	**2**	green plates	238.5 (dec)[d]	854, 746	798, 731	803, 733	807, 733	803, 732	0.50
$\mathbf{I}_3$–3CNQ	**3a**	green blocks	235.2 (dec)[d]						
	3b	golden blocks	236.6 (dec)[d]	852, 744	800, 732	805, 734	809, 736	806, 733	0.50
	3c	green needles	237.0 (dec)[d]	858, 746[f]					
	3d	green blocks	237.5 (dec)[d]						
$\mathbf{I}_4$–3CNQ	**4**	green plates	232.7 (dec)[d]	848, 748	799, 732	805, 734	809, 735	806, 734	0.50
$\mathbf{I}_5$–3CNQ	**5**	green plates	194.8	834, 744	800, 732	805, 734	808, 735	806, 734	0.50
$\mathbf{I}_6$–3CNQ	**6a**	green plates	195.8	852, 748					
	6b	green rods	195.8	844, 748	800, 732	805, 734	809, 735	805, 734	0.50
	6c	golden blocks	196.3	844, 750					
$\mathbf{I}_7$–3CNQ	**7a**	green plates	189.5	858, 746	799, 733	805, 734	809, 735	805, 733	0.50
	7b	golden blocks	184.7	844, 750					
$\mathbf{I}_8$–3CNQ	**8**	green blocks	161.3	850, 756	801, 733	805, 734	809, 735	804, 734	0.50
$\mathbf{I}_{10}$–3CNQ	**10**	green blocks	148.1	842, 746	800, 733	806, 735	809, 736	805, 734	0.50
$\mathbf{I}_{14}$–3CNQ	**14**	golden powder	124.2	846, 754	800, 732	806, 734	810, 737	805, 735	0.51
$\mathbf{I}_{16}$–3CNQ	**16**	green powder	101.8	842, 754	801, 733	806, 734	810, 736	805, 734	0.50
$\mathbf{I}_{18}$–3CNQ	**18**	golden powder	95.4	854, 752	801, 733	806, 735	809, 736	806, 735	0.50
$\mathbf{I}_{20}$–3CNQ	**20**	golden plates	102.7	852, 758	800, 733	806, 735	810, 736	805, 734	0.50
$\mathbf{I}_{22}$–3CNQ	**22**	brass powder	107.2	850, 754	801, 733	806, 734	809, 736	806, 734	0.50

a) Letters **a**–**d** for **3**, **6**, and **7** show polymorphism. b) Measured by DSC. c) Decomposition before melting. d) Decomposition immediately after melting. e) Peak positions. f) **3b**–**3d** mixture.

ses were collected using a Bruker AXS DIP-2020K oscillator type X-ray imaging plate with monochromated Mo Kα (λ = 0.71073 Å, 1 Å = 0.1 nm) radiation at room temperature. Structures were determined by a direct method using SHELXS-97.[21] Least-squares refinements were performed by the full-matrix least-squares method on F^2 with SHELXL-97.[22] All non-hydrogen atoms were refined anisotropically. The hydrogen atoms were included without refinement. The positions of the hydrogen atoms were calculated assuming sp^3 or sp^2 conformations of the carbon atoms. Crystallographic data have been deposited with the Cambridge Crystallographic Data Centre: Deposition numbers CCDC-680492–680504. Copies of the data can be obtained free of charge via http://www.ccdc.cam.ac.uk/conts/retrieving.html (or from the Cambridge Crystallographic Data Centre, 12, Union Road, Cambridge, CB2 1EZ, UK; Fax: +44 1223 336033; e-mail: deposit@ccdc.cam.ac.uk). Crystallographic data are summarized in Supporting Information.

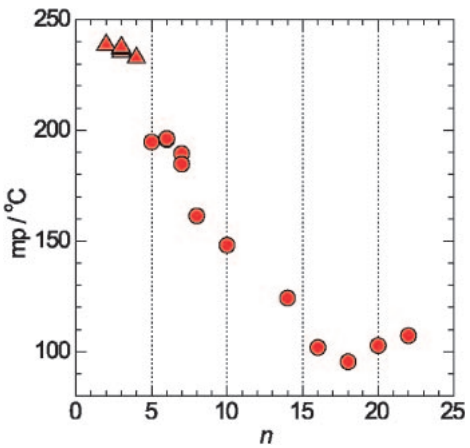

Figure 1. Plot of melting point vs. alkyl chain length (n) for $\mathbf{I}_n$–3CNQ. Compounds shown by triangles decomposed just after melting.

Results and Discussion

Thermal Properties of $\mathbf{I}_n$–3CNQ. Melting Points: Figure 1 shows a plot of the melting points of $\mathbf{I}_n$–3CNQ against alkyl chain length (n). The melting point decreased steadily from 238.5 °C with increasing n in the range $2 \leq n \leq 18$, then increased after it reached the minimum point at $n = 18$ (mp: 95.4 °C). Such behavior has also been observed for TTF derivatives having long alkylchalcogeno groups (TXC_n-TTF); melting point decreases with increasing n and increases monotonously after reaching the minimum point at $n = 4$ for TTC_n-TTF,[19c] $n = 5$ for $TSeC_n$-TTF,[19d] and $n = 6$ for $TTeC_n$-TTF.[19e] In the crystal structures of TTC_n-TTF, π–π interaction of the TTF moiety and self-aggregation ability originating from intermolecular van der Waals interactions associated with alkyl chains are competitive, and the former is dominant in the short alkyl chain compounds ($n \leq 4$), while the latter is dominant for the long alkyl chain compounds ($n > 5$).[19a] Therefore, it is plausible that the self-aggregation ability of alkyl chains become more prominent than the interaction of π-moieties (π–π and/or dipole–dipole interactions) for $\mathbf{I}_n$–3CNQ when $n > 18$. In fact, in the crystal structure of $\mathbf{I}_{20}$–3CNQ, the long alkyl chain exhibited a self-assembling property to form forming a layered structure (vide infra).

Supercooled Form: The color of the crystal was either green or golden as shown in Figure 2 (green crystals for $\mathbf{I}_2$–3CNQ (**2**) and golden for $\mathbf{I}_3$–3CNQ (**3b**)). Even though their colors differed, no significant differences were observed in their UV–vis absorption spectra (Table 1, refer Supporting Information).

DSC data for $\mathbf{I}_{20}$–3CNQ with a fast heating/cooling rate of

10 K min^{-1} indicated that it began to melt at 102.7 °C. In the first cooling process down to 50 °C, the second heating, and the second cooling processes, no exo- and endothermic changes were observed (see Supporting Information). Figure 3a shows the DSC data for $\mathbf{I}_{20}$–3CNQ with a 1 K min^{-1} heating/cooling rate. The X-ray powder pattern (Figure 3b) for the purple liquid formed after the first cooling process (stage 2 in Figure 3a, curve 2 in Figure 3b) showed amorphous pattern characteristics of a supercooled fluid. The second heating process induced a broad and exothermic crystallization from 55 °C and melting at 88.2 °C, which is considerably lower than that of the original $\mathbf{I}_{20}$–3CNQ crystal (stage 3 in Figure 3a). The X-ray powder pattern at stage 3 in Figure 3a (curve 3 in Figure 3b) differed from that of the virgin sample (stage 1 in Figure 3a, curves 1 and 4 in Figure 3b), indicating that the supercooled fluid crystallized to a different phase from the original. The second cooling process also displayed supercooled state characteristics. The supercooled fluid state was observed for all $n \geq 6$ derivatives (see Supporting Information).

After melting, the golden solid (Figure 4a) transformed into a highly viscous liquid with a reddish purple color, and the supercooled fluid could be easily handspun into wires with diameters less than 100 μm (Figure 4b). The fluid wires transform into crystalline wires after annealing at 70 °C recovering the gold colored luster (Figure 4c) which melted at ca. 90 °C (stage 3 in Figure 3a). In the solid-state UV–vis spectrum, the crystalline sample of $\mathbf{I}_{20}$–3CNQ showed absorption bands at 11.7×10^3 (A), 13.2×10^3 (B), and $\approx 15 \times 10^3$ cm^{-1} (C) (curve 1 in Figure 4d). The spectrum of the supercooled fluid state was identical to that of the crystal state (curve 2 in Figure 4d); however, a new low-lying absorption band was observed at approximately 1000 nm in the supercooled fluid state (band-S indicated by an arrow). The band-S was absent in the recovered solid (curve 3 in Figure 4d).

Solution-State Properties. Electrochemical Properties: Cyclic voltammograms were measured for the $\mathbf{I}_n$–3CNQ ($n = 1$, 3, 6, and 20) derivatives. They exhibited irreversible oxidation and reduction ($E_p^{ox} = +0.57$ and $E_p^{red} = -0.45$ V for $n = 1$; $E_p^{ox} = +0.60$ and $E_p^{red} = -0.40$ V for $n = 3$; $E_p^{ox} = +0.60$ and $E_p^{red} = -0.41$ V for $n = 6$; $E_p^{ox} = +0.61$ and $E_p^{red} = -0.42$ V for $n = 20$, V vs. SCE) (Figure 5 for $n = 1$, refer Supporting Information for other compounds). The oxidation and reduction potentials scarcely depended on the alkyl chain length, indicating that the alkyl chain length does not affect the electron-donating and -accepting abilities of the indoline and 3CNQ moieties, respectively.

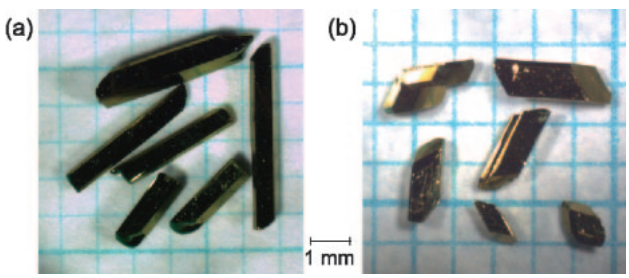

Figure 2. Single crystals of (a) $\mathbf{I}_2$–3CNQ (**2**) and (b) $\mathbf{I}_3$–3CNQ (**3b**).

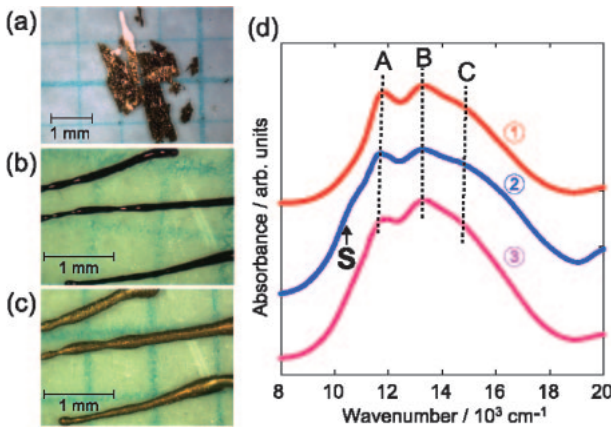

Figure 4. Images of (a) a crystalline sample of $\mathbf{I}_{20}$–3CNQ, (b) supercooled liquid spun into a wire, and (c) crystalline wires annealed at 70 °C. (d) Absorption spectra of $\mathbf{I}_{20}$–3CNQ dispersed in KBr: (1) crystalline sample, (2) supercooled state (heated to 120 °C and then cooled to room temperature), and (3) annealed sample. Bands-A–C were observed in all states, and a shoulder peak (band-S) appeared in the supercooled state, indicated by an arrow.

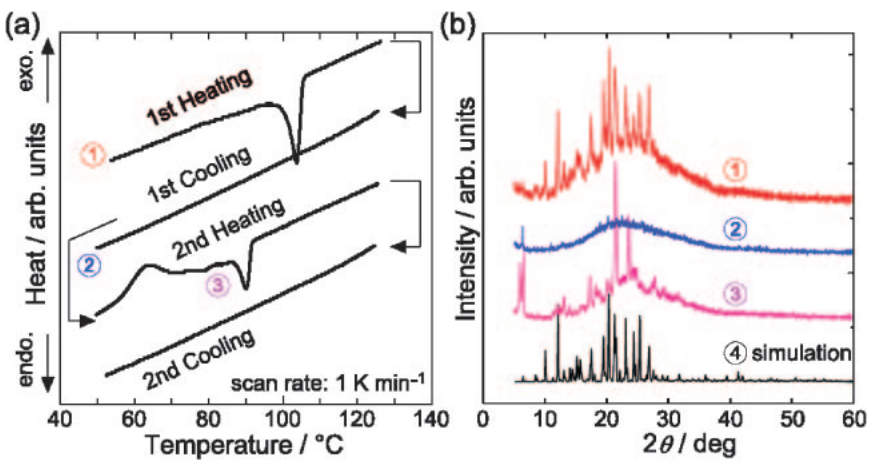

Figure 3. (a) DSC measurements for $\mathbf{I}_{20}$–3CNQ with a scanning speed of 1 K min^{-1}. (b) X-ray powder diffraction patterns of $\mathbf{I}_{20}$–3CNQ, where curves 1–3 indicate the stages in (a), and curve 4 describes the simulated pattern from the crystal structure analysis.

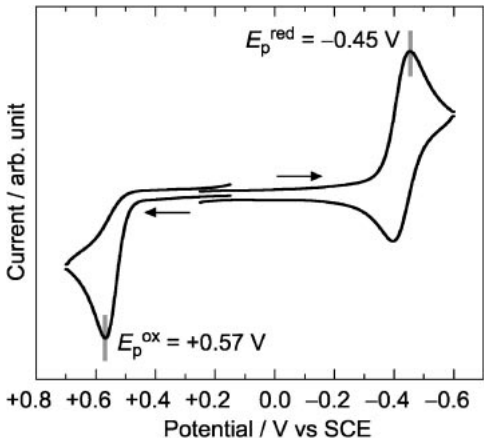

Figure 5. Cyclic voltammogram of $\mathbf{I}_1$–3CNQ. Experimental conditions: solvent, MeCN containing 0.1 M *n*-$Bu_4N^+BF_4^-$; scan rate, 50 mV s^{-1}; reference electrode, SCE.

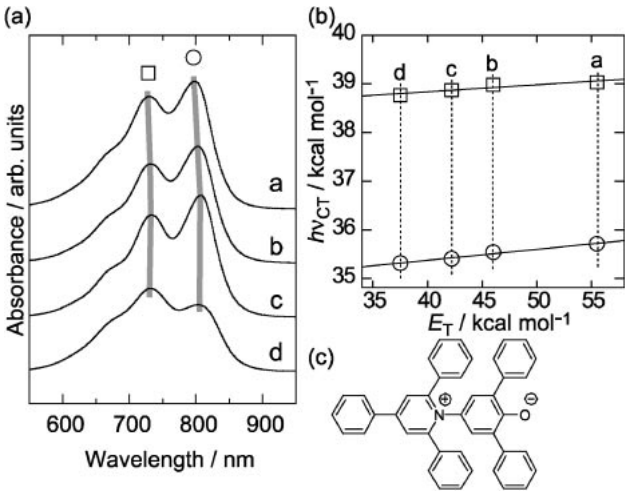

Figure 6. (a) UV–vis spectra of $\mathbf{I}_2$–3CNQ in various solvents (a: MeOH (E_T = 55.5), b: MeCN (46.0), c: acetone (42.2), and d: PhCl (37.5)). Gray lines indicate the shift of peaks. (b) Plots of transition energies of $\mathbf{I}_2$–3CNQ against E_T values. Labels a–d are measurement solvents. (c) Chemical structure of Reichardt's betaine dye.[24]

Absorption Spectra and Degree of CT in Solution: $\mathbf{I}_n$–3CNQ compounds exhibited intense and multiple absorptions at 600–900 nm ascribable as an intramolecular CT band in the solution state, which showed a slight blue solvatochromic shift of 3–15 nm from PhCl to MeOH in each compound (peaks marked by a circle and square, Figure 6a).

The intramolecular CT energy ($h\nu_{CT}$) of $D^{\delta+}$–π–$A^{\delta-}$ is expressed by eq 1,[23] where ε, r, ΔG, $2X$, and C are the dielectric constant of the solvent, average distance between the D and A moieties, difference in the solvation energies of D^0–π–A^0 and D^{1+}–π–A^{1-} species, resonance stabilization energies of D^0–π–A^0 and D^{1+}–π–A^{1-} species, and Coulomb term, respectively.

$$h\nu_{CT}\ (D^{\delta+}\text{–}\pi\text{–}A^{\delta-}) = (2\delta - 1)\left(\frac{1}{\varepsilon}\frac{e^2}{r} - \Delta G\right) + (2X - C) \quad (\delta > 0.5) \qquad (1)$$

In the previous paper,[18] we evaluated δ of $\mathbf{I}_1$–3CNQ-R by normalizing it with the $\mathbf{I}_1$–3CNQ-F_4 molecule assuming a completely ionic compound ($\delta = 1$); however, as shown in the estimations of δ in the solid state (vide infra), the δ value of $\mathbf{I}_1$–3CNQ-F_4 is not 1. In this study, we employed Reichardt's betaine dye (Figure 6c) since its completely ionic state ($\delta = 1$) is comfirmed.[24] The intramolecular CT energy of Reichardt's dye (E_T), which is frequently used as an indicator of solvent polarity, also follows eq 1 and is expressed as

$$h\nu_{CT}\ (\text{Reichardt's dye}) = \left(\frac{1}{\varepsilon}\frac{e^2}{r} - \Delta G'\right) + (2X - C) = E_T \qquad (2)$$

The $h\nu_{CT}$ values of the $\mathbf{I}_n$–3CNQ derivatives in various solvents showed a linear dependence on Reichardt's E_T values (Figure 6b) expressed as

$$h\nu_{CT}\ (D^{\delta+}\text{–}\pi\text{–}A^{\delta-}) = aE_T + b = a\left(\frac{1}{\varepsilon}\frac{e^2}{r} - \Delta G'\right) + a(2X - C) + b \qquad (3)$$

Accordingly, the slope a of a linear line in the plot of $h\nu_{CT}$ vs. E_T gives the δ value (δ_{solv}) by

$$a = 2\delta_{solv} - 1 \qquad (4)$$

In the estimation of δ_{solv}, the second lowest energy peak was used, because the band was the most intense and could be clearly observed. It should be noted that the obtained δ_{solv} values bear some ambiguities due to the difference in the solvation energies (ΔG) between Reichardt's betaine dye and $\mathbf{I}_n$–3CNQ compounds. However, since the difference in ΔG values should be small compared to whole intramolecular CT energy, and the linear relationship between a and δ values is confirmed, the δ_{solv} value is a good parameter to express degree of CT of $\mathbf{I}_n$–3CNQ compounds in the solution state.

The estimated δ_{solv} values for all $\mathbf{I}_n$–3CNQ are summarized in Table 1. The δ_{solv} value of $\mathbf{I}_1$–3CNQ (0.51) looks slightly larger than those of $n \geq 2$ compounds; however, significant dependence of the δ_{solv} value on alkyl chain length was not found. The effect of alkyl chain was more clearly seen in the peak position of intramolecular CT bands. The second lowest peaks in MeCN showed a low-energy shift from 725 nm for $n = 1$ to 733 nm $n = 2$ (Figure 7), indicating the decrement of δ according to eq 1. Similar behavior was observed in the other solvents (Table 1). Further increments of alkyl chain length did not affect the peak positions (Figure 7 and Table 1). This relationship between δ and alkyl chain length can be explained by molecular conformation as follows.

For an $\mathbf{I}_n$–3CNQ molecule, two molecular conformations, namely Type I and II, in which the *N*-alkyl group located close to and far from the CN1 group, respectively, can be expected (Scheme 2). In a molecule of Type I conformation, the negatively charged CN1 group is close to the π-electronic system of the indoline moiety and attracts a positive charge on the D part to enhance the intramolecular CT. Such effect becomes weak for a molecule of Type II conformation. Accordingly, a molecule of Type I conformation is expected to have a larger δ value than that of Type II. This hypothesis was confirmed by the estimations of δ values in the solid state (vide infra). The conformation of an $\mathbf{I}_n$–3CNQ molecule is determined by the

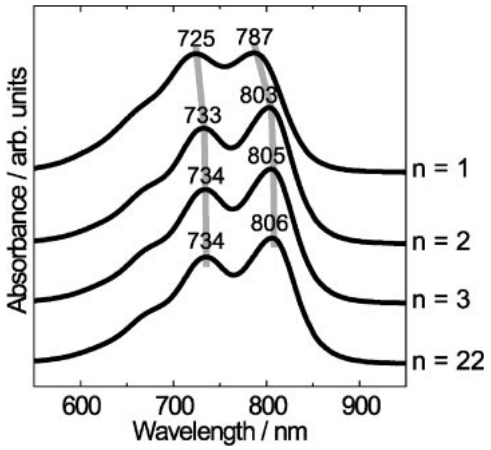

Figure 7. UV–vis spectra of $\mathbf{I}_n$–3CNQ ($n = 1$, 2, 3, and 22) in MeCN. Gray lines indicate the shifts of peaks.

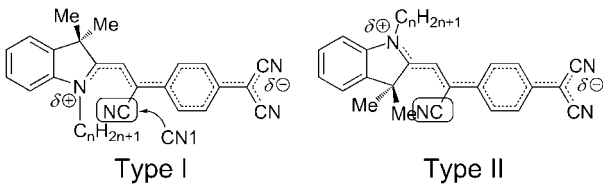

Scheme 2. Two kinds of conformational isomers of $\mathbf{I}_n$–3CNQ (Types I and II).

balance of steric repulsion between the 3,3-dimethyl group in the indoline moiety and the CN1 group, and that between the *N*-alkyl chain and the CN1 group. With increasing alkyl chain length, steric repulsion between the *N*-alkyl chain and CN1 group becomes larger, and the contribution of Type I conformation which gives larger δ decreases. The larger $h\nu_{CT}$ value of $\mathbf{I}_1$–3CNQ reflects the contribution of Type I conformation, while the nearly constant $h\nu_{CT}$ values of $\mathbf{I}_n$–3CNQ ($n \geq 2$) indicate that the Type II conformation is dominant for them in the solution state. Since the contributions of Type I and II molecules to the $h\nu_{CT}$ values are mixed in the solution state, the dependence of δ_{solv} value on alkyl chain length was considerably smaller than the differences of δ values between Type I and II conformations in the solid state (vide infra).

Molecular and Crystal Structures of $\mathbf{I}_n$–3CNQ Derivatives. In the crystal structures, two molecular conformations, Type I and II, were observed. The molecular conformations and dihedral angles (θ_1–θ_3) of the D and A moieties in the crystal structures of $\mathbf{I}_n$–3CNQ derivatives ($n = 2$–8, 10, and 20) are summarized in Table 2. Dihedral angles between the benzenoic ring in the 3CNQ moiety, and terminal dicyanomethylene group and cyanoethene π-bridge are indicated by θ_1 or θ_2, respectively. The dihedral angle (θ_3) between the least squares fitting planes of the indoline moiety and the cyanoethene π-bridge distinguishes Types I ($\theta_3 < 90°$) and II ($\theta_3 > 90°$) (Table 2).

$\mathbf{I}_2$–3CNQ (2): **2** was obtained by recrystallization from MeCN and crystallized in a monoclinic system. In this crystal, one $\mathbf{I}_2$–3CNQ molecule, which had a Type II conformation ($\theta_3 = 154.1°$), was crystallographically independent (Figures 8a and 8b). The 3CNQ moiety stacked with interplanar distances of 3.41 and 3.66 Å to form a one-dimensional π-stacking column along the *a* axis (yellow areas in Figure 8c). The 3CNQ stacks were twisted by 49°, and the overlap between neighboring 3CNQ moieties was small (Figure 8d). The indoline moiety formed a dimerized unit with a large interplanar distance (4.65 Å) (red areas in Figures 8c and 8d).

Table 2. Molecular Conformations and Dihedral Angles of $\mathbf{I}_n$–3CNQ Molecules[a)]

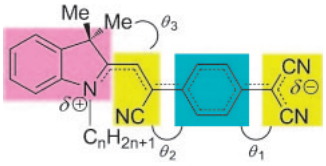

Compounds[b)]		Type	Dihedral angle/°		
			θ_1	θ_2	θ_3
$\mathbf{I}_2$–3CNQ	**2**	II	4.7	3.2	154.1
$\mathbf{I}_3$–3CNQ	**3a**	I	2.2	4.5	45.4
	3b	II	3.8	2.2	174.0
$\mathbf{I}_4$–3CNQ	**4**	II	8.3	7.4	174.9
$\mathbf{I}_5$–3CNQ	**5**	II	7.0	3.1	175.0
$\mathbf{I}_6$–3CNQ	**6a**	II	1.3	4.2	155.9
	6b	II	1.5	4.5	156.1
	6c	II	2.4	9.7	161.2
$\mathbf{I}_7$–3CNQ	**7a^{I}**	II	3.9	3.6	156.6
	7a^{II}	II	1.0	4.1	154.0
	7b	II	2.1	4.5	150.1
$\mathbf{I}_8$–3CNQ	**8^{I}**	II	5.5	3.6	170.5
	8^{II}	II	2.4	9.1	151.5
$\mathbf{I}_{10}$–3CNQ	**10**	I	5.2	7.9	49.3
$\mathbf{I}_{20}$–3CNQ	**20^{I}**	II	3.4	1.9	158.0
	20^{II}	II	1.2	9.1	165.2

a) The indoline moiety (red part in the molecular structure) is defined by one nitrogen and eight carbon atoms, and does not include the alkyl chain and two methyl groups. b) Symbols I and II in **7a**, **8**, and **20** indicate crystallographically independent molecules in one crystal.

($\mathbf{I}_3$–3CNQ)(MeCN) (3a): **3a** was obtained by recrystallization from MeCN and crystallized in a triclinic system, where one $\mathbf{I}_3$–3CNQ and one MeCN molecule were crystallographically independent. In this crystal, the $\mathbf{I}_3$–3CNQ molecule had a Type I conformation, where the indoline and 3CNQ moieties are twisted by $\theta_3 = 45.4°$ (Figure 9a). The 3CNQ moiety was flat ($\theta_1 = 2.2°$ and $\theta_2 = 4.5°$), and the alkyl chain was extended nearly perpendicular to the indoline plane to reduce steric repulsion with the CN1 group (Figure 9a). In the crystal structure, both the 3CNQ and indoline moieties formed dimer units with interplanar distances of 3.39 and 3.50 Å, respectively (yellow and red areas, respectively, in Figure 9b). Both dimers had head-to-tail stacking to cancel the dipole moment (Figures 9b and 9c). 3CNQ dimers were isolated by MeCN molecules.

($\mathbf{I}_3$–3CNQ)($\mathbf{C_6H_6}$)$_{0.5}$ (3b): **3b** was obtained by recrystallization from benzene/hexane and crystallized in a triclinic system. One $\mathbf{I}_3$–3CNQ molecule and half of a benzene molecule with an inversion center were crystallographically independent. The $\mathbf{I}_3$–3CNQ molecule in **3b** had a Type II conformation, where indoline and 3CNQ moieties were nearly parallel ($\theta_3 = 174.0°$) (Figure 10a). The dihedral angles θ_1 and θ_2 were 3.8 and 2.2°, respectively, and the molecule had a planar

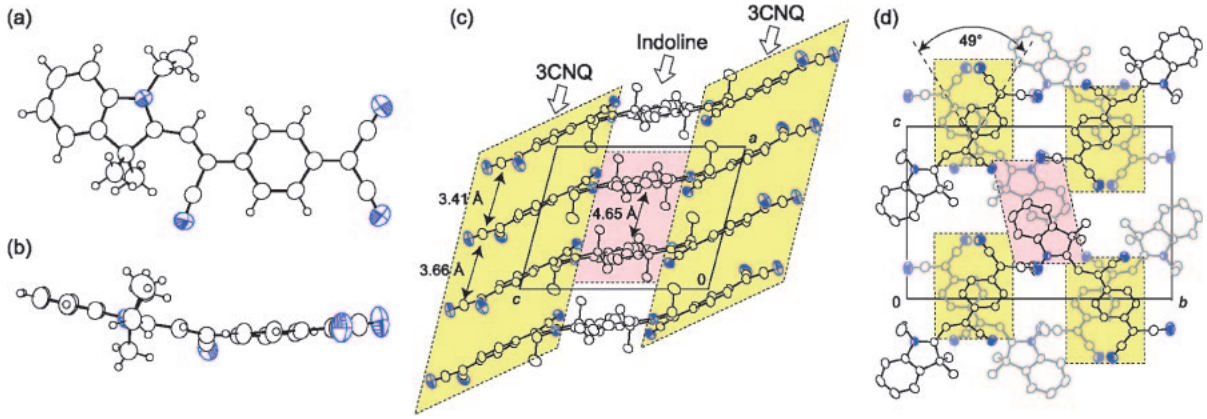

Figure 8. Molecular structure of $\mathbf{I}_2$–3CNQ in **2**; (a) top view and (b) side view. (c) The *b* axis projection of **2** showing the π-stacking columns of the 3CNQ moieties (yellow areas). (d) The *a* axis projection of **2** showing the overlap patterns on 3CNQ and indoline moieties (yellow and red areas, respectively). Hydrogen atoms are omitted in (c) and (d).

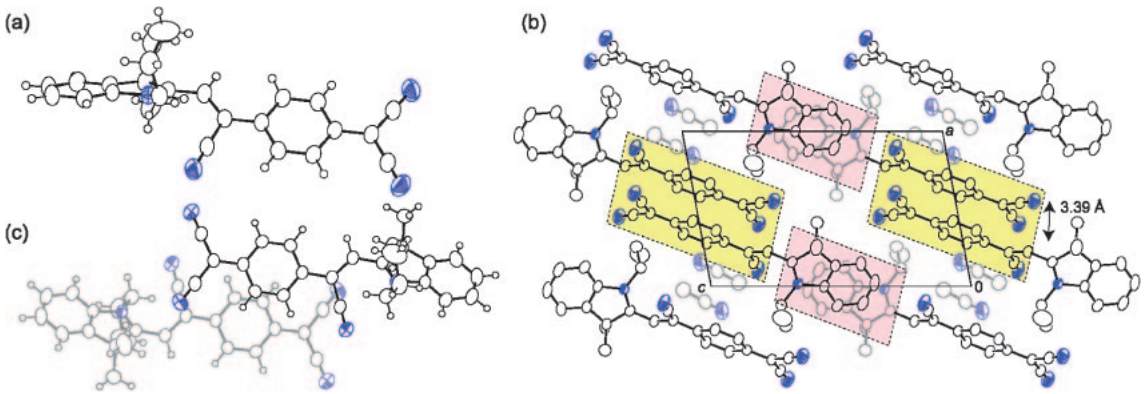

Figure 9. (a) Molecular structure of $\mathbf{I}_3$–3CNQ in **3a**. (b) The *b* axis projection of **3a**. Yellow and red areas show dimer units of 3CNQ and indoline moieties, respectively. Light colored molecules are MeCN solvents. Hydrogen atoms are omitted in (b). (c) Overlap mode of a 3CNQ dimer.

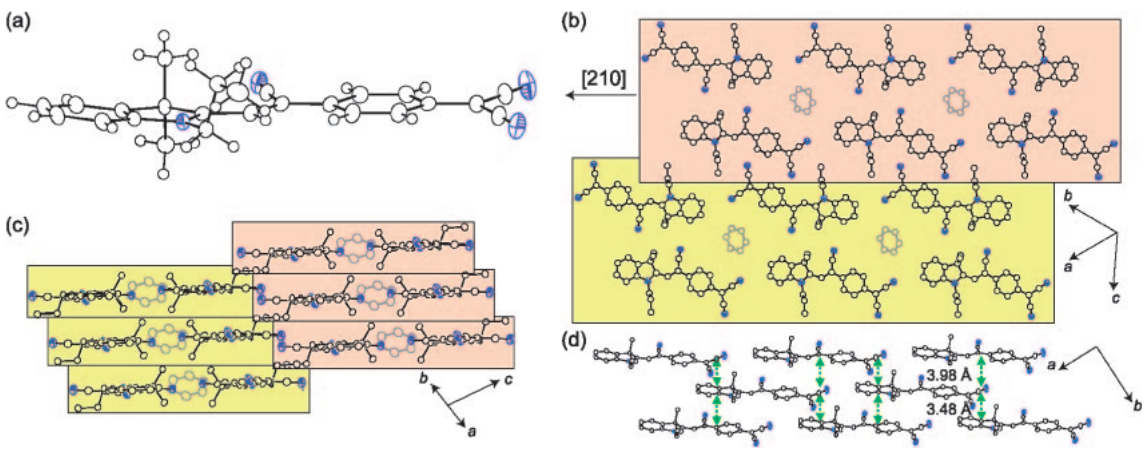

Figure 10. (a) Molecular structure of $\mathbf{I}_3$–3CNQ in **3b**. Molecular packing of **3b** viewed (b) perpendicular to the molecular plane and (c) along the molecular long axis. Orange and yellow areas represent the ribbon-like sheet structures, and the light colored molecules are benzene solvents. (d) The two-dimensional π-stacking structure of $\mathbf{I}_3$–3CNQ viewed along the *c* axis. Hydrogen atoms are omitted in (b)–(d).

structure with a small maximum deviation (0.23 Å) from the least-squares plane of the entire molecular structure (excluding propyl and dimethyl groups). These flat molecules formed a ribbon-like sheet with a width of two molecules along the [210] direction (Figures 10b and 10c), and these sheets stacked uniformly along the *a* axis (Figure 10c). Molecular dipoles in **3b** cancelled out by the formation of molecular pairs in a side-by-side orientation (Figure 10b). The $\mathbf{I}_3$–3CNQ molecule

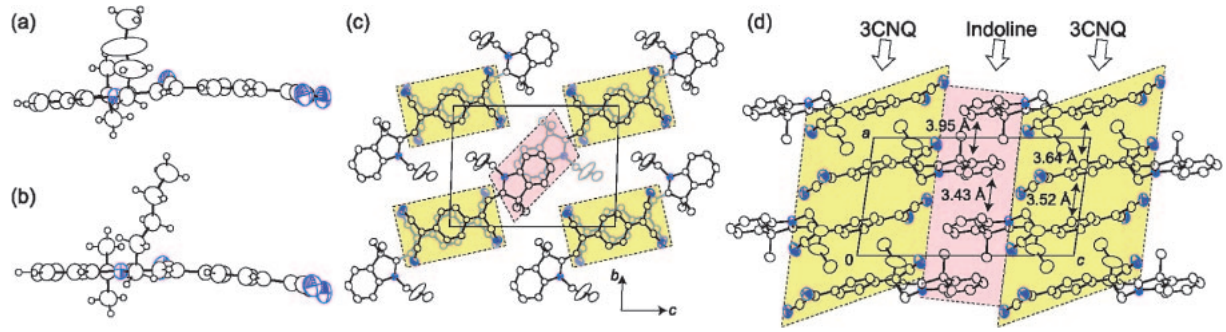

Figure 11. Side views of molecular structures of (a) I_4–3CNQ (**4**) and (b) I_5–3CNQ (**5**). Molecular packing of **4** viewed along (c) the *a* axis and (d) *b* axis. Yellow and red areas represent the π-stacking columns of 3CNQ and indoline moieties, respectively. Hydrogen atoms are omitted in (c) and (d). **4** and **5** were iso-structural.

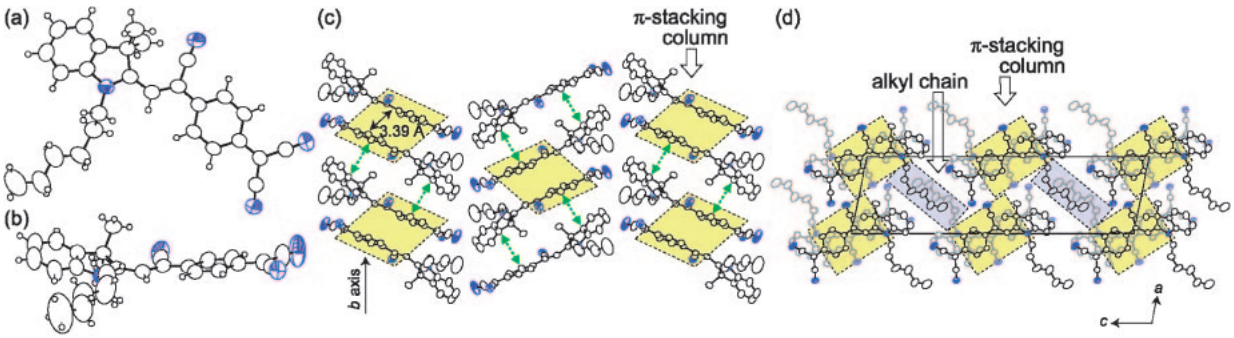

Figure 12. Molecular structure of I_6–3CNQ (**6a**); (a) top view and (b) side view. (c) Crystal packing of **6a** viewed along the molecular short axis, showing the one-dimensional π-stacking columns. (d) The *b* axis projection of **6a**. The π-stacks of 3CNQ moieties and aggregation of alkyl chains are represented by the yellow and blue boxes, respectively, and the green arrows in (c) represent the π–π interactions between indoline and 3CNQ moieties in a column. Hydrogen atoms are omitted in (c) and (d).

formed π–π interactions between indoline and 3CNQ moieties with interplanar distances of 3.48 and 3.98 Å, forming a two-dimensional sheet (green arrows in Figure 10d).

I_4–3CNQ (4) and I_5–3CNQ (5): Both **4** and **5** were obtained by recrystallization from MeCN and were iso-structures. They crystallized in a triclinic system, and one molecule was crystallographically independent in each crystal. Both I_4–3CNQ and I_5–3CNQ molecules had a Type II conformation with a flat molecular shape ($\theta_3 = 174.9°$ for **4** and 175.0° for **5**, Figures 11a and 11b). The alkyl group of each molecule extended nearly perpendicular to the molecular plane. In the crystal structure of **4**, both 3CNQ and indoline moieties formed segregated stacks along the *a* axis (yellow and red areas, respectively, in Figures 11c and 11d) with interplanar distances of 3.52 and 3.64 Å for the 3CNQ column, and 3.43 and 3.95 Å for the indoline column. Both dimers showed head-to-tail stacking with an inversion center to cancel the dipole moment. Similarly to **4**, **5** had segregated stacks of 3CNQ and indoline moieties, where the interplanar distances in the 3CNQ column were nearly uniform (3.55 Å) while indolines were dimerized (3.45 and 3.89 Å).

I_6–3CNQ (6a–6c) and I_7–3CNQ (7a and 7b): Three polymorphs were found for I_6–3CNQ, two of which **6a** and **6b** were obtained by recrystallization from benzene/hexane and were included in the same batch: the other polymorph **6c** was obtained by recrystallization from MeCN as a solvated crystal. In the case of I_7–3CNQ, two polymorphs were obtained from the same batch, which was obtained by recrystallization from benzene/hexane.

Crystals **6a**, **6b**, **7a**, and **7b** had very similar structures and crystallized in monoclinic space groups except for **7b**, which was in a triclinic system. In all cases, I_n–3CNQ molecules had a Type II conformation, and dihedral angles of all the molecules were very similar ($\theta_3 = 150.1$–$156.6°$, $\theta_1 = 1.0$–$3.9°$, and $\theta_2 = 3.6$–$4.5°$, Table 2 and Figures 12a and 12b). The alkyl group of each molecule extended nearly perpendicular to the molecular long axis and parallel to the molecular plane (Figure 12a). In the crystal structure of **6a**, the 3CNQ moiety stacked in a head-to-tail manner with an interplanar distance of 3.39 Å (yellow area in Figure 12c). In addition, π–π interactions were formed between indoline and 3CNQ moieties (face-to-face distance: 3.5–4.3 Å, green arrows), resulting in the formation of a one-dimensional columnar structure along the *b* axis (Figure 12c). Inversion centers were located at the centers of each π–π interaction to cancel the molecular dipole moments. Because of the self-assembling ability of the alkyl chains, a one-dimensional motif parallel to the D–π–A column (*b* axis) was formed. This one-dimensional motif of alkyl chains was included in a channel surrounded by the D–π–A columns (blue areas in Figure 12d). In the crystal structures of **6b**, **7a**, and **7b**, one-dimensional structures similar to that of **6a** formed by π-stacking self-aggregation of alkyl chains were observed.

6c crystallized in a monoclinic space group and included a MeCN solvent molecule. The I_6–3CNQ molecule in **6c** had a Type II conformation and a similar planarity to those of **6a** and

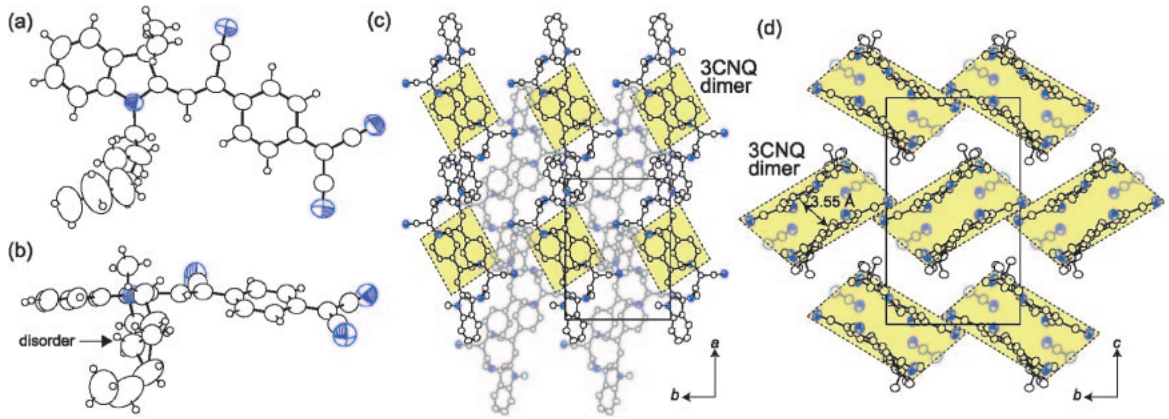

Figure 13. Molecular structure of $\mathbf{I}_6$–3CNQ (**6c**); (a) top view and (b) side view. The third carbon atom of the alkyl chain disordered into two positions with site occupancy factors of 0.733 and 0.267, respectively. (c) The *c* axis projection of **6c**, where molecules on the $c = 1/2$ plane are represented by light colors. (d) The *a* axis projection of **6c**, where light colored molecules are MeCN solvents. π-Stacks of 3CNQ moieties are indicated by the yellow areas, and hydrogen atoms and alkyl chains are omitted in (c) and (d).

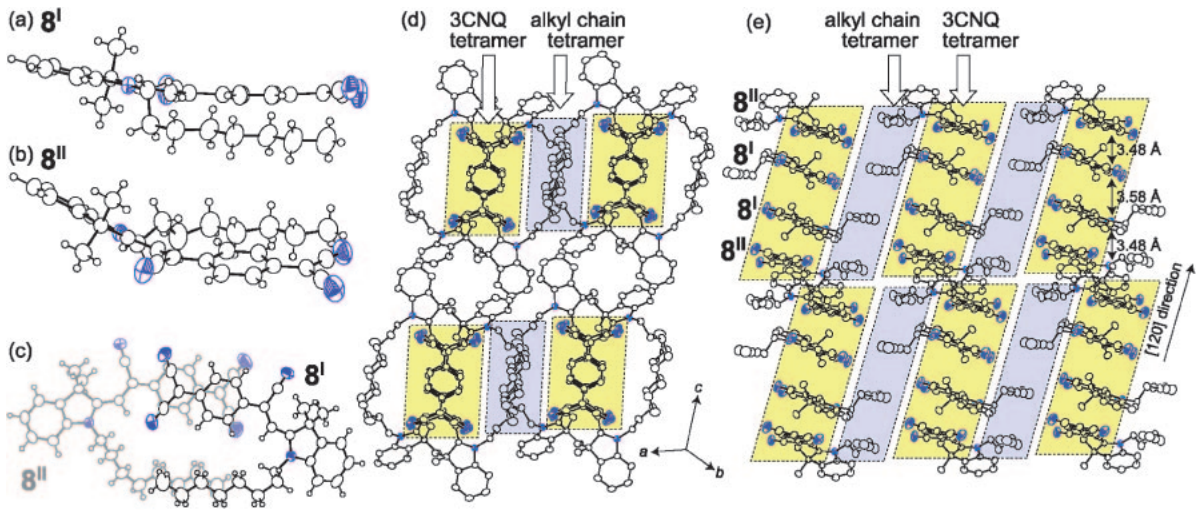

Figure 14. (a and b) Molecular structures of $\mathbf{I}_8$–3CNQ ($\mathbf{8^I}$ and $\mathbf{8^{II}}$, respectively). (c) Overlap pattern of an $\mathbf{8^I}$–$\mathbf{8^{II}}$ dimer. The light colored molecule is $\mathbf{8^{II}}$. The crystal packing of **8** viewed along (d) the π-stacking direction and (e) molecular long axis. π-Stacks of 3CNQ moieties and aggregation of alkyl chains are represented by yellow and blue areas, respectively. Hydrogen atoms and benzene solvents are omitted in (d) and (e).

6b except for the slightly larger θ_2 ($\theta_3 = 161.2°$, $\theta_1 = 2.4°$, and $\theta_2 = 9.7°$, shown in Table 2 and Figures 13a and 13b). The alkyl group extended nearly perpendicular to the molecular short axis and parallel to the molecular plane (Figure 13a). In the crystal structure, the 3CNQ moiety stacked with an interplanar distance of 3.55 Å, forming a dimer unit (yellow areas in Figure 13c). Inversion centers were located at the center of the dimer to cancel the molecular dipole moments. The dimers were arranged in a herring-bone structure, and no intermolecular interactions, such as π–π interaction and aggregation of alkyl chains, were present between the dimers (Figure 13d).

$(\mathbf{I_8}$–3CNQ$)(\mathbf{C_6H_6})_{0.5}$ (8): The solvated crystal **8** crystallized in a triclinic system. Two $\mathbf{I}_8$–3CNQ ($\mathbf{8^I}$ and $\mathbf{8^{II}}$) and one benzene molecules are crystallographically independent. Both $\mathbf{8^I}$ and $\mathbf{8^{II}}$ had a Type II conformation with $\theta_3 = 170.5$ and 151.5°, respectively (Figures 14a and 14b). Alkyl chains of both molecules extended nearly parallel to the long axis of 3CNQ moieties. A head-to-tail π-stack of 3CNQ moieties between two $\mathbf{8^I}$ and $\mathbf{8^{II}}$ formed a dimerized structure in which two alkyl chains were bound to each other (Figure 14c). The interplanar distance of the dimer was 3.48 Å. This dimer unit stacked with an interplanar distance of 3.58 Å to form an $\mathbf{8^{II}}$–$\mathbf{8^I}$–$\mathbf{8^I}$–$\mathbf{8^{II}}$ tetramer unit at the center of which an inversion center was located (yellow areas in Figures 14d and 14e). Alkyl chains also aggregated to form a tetramer (blue areas in Figures 14d and 14e). These tetramer units stacked alternately to form a column along the [120] direction.

$\mathbf{I_{10}$–3CNQ (10): Crystal **10** was obtained by recrystallization from benzene and crystallized in a triclinic system. There was one crystallographically independent $\mathbf{I}_{10}$–3CNQ molecule. Contrary to other $\mathbf{I}_n$–3CNQ molecules having long alkyl chains, $\mathbf{I}_{10}$–3CNQ in this crystal had a Type I conformation with $\theta_3 = 49.3°$, and the CN groups deviated from the

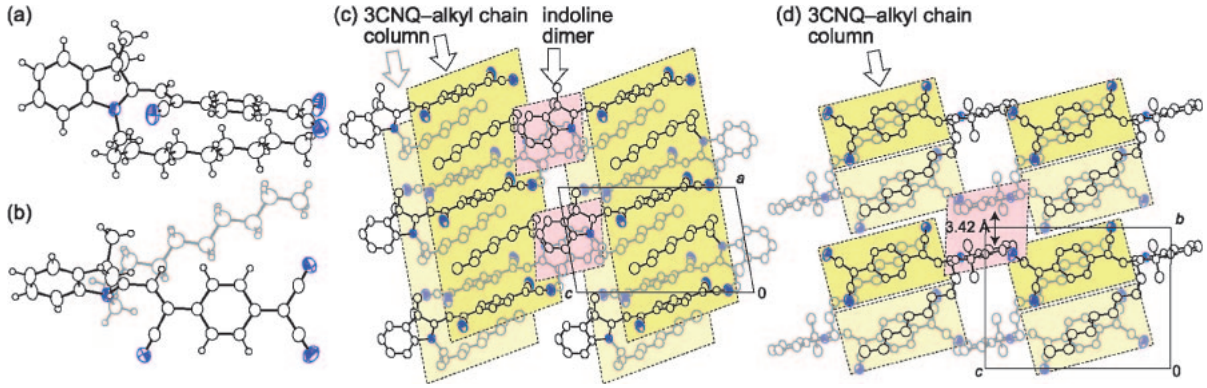

Figure 15. Molecular structure of $\mathbf{I}_{10}$–3CNQ (**10**); (a) side view and (b) top view. The alkyl chain is represented by the gray-colored atoms. The (c) *b* axis and (d) *a* axis projections of **10**. The 3CNQ–alkyl chain columns and π-stacks of the indoline moiety are indicated by the yellow and red areas, respectively. Light colored molecules in (c) belong to the next column along the *b* axis. Hydrogen atoms are omitted in (c) and (d).

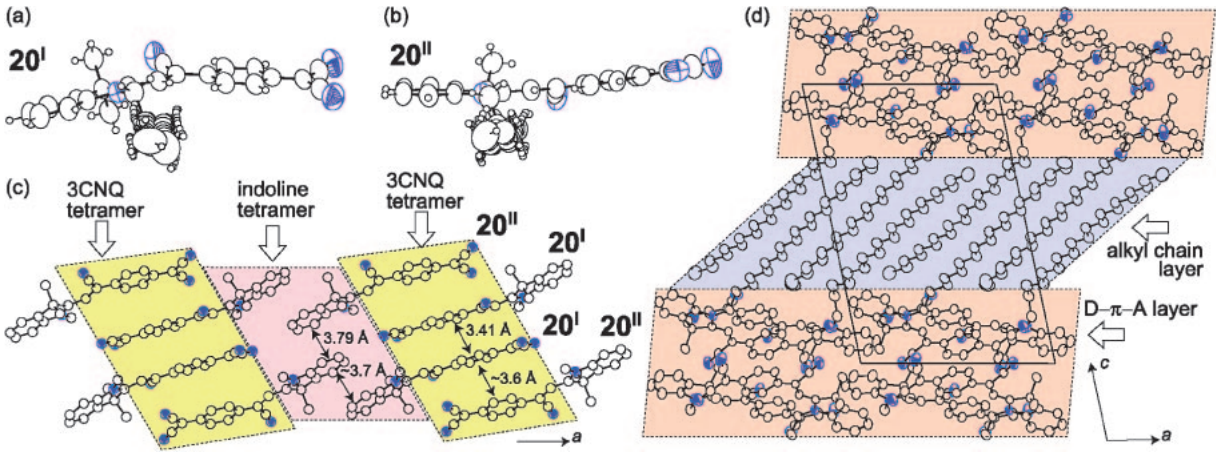

Figure 16. (a and b) Side views of molecular structures of $\mathbf{I}_{20}$–3CNQ ($\mathbf{20^I}$ and $\mathbf{20^{II}}$, respectively). (c) D–π–A ribbon structure, where 3CNQ and indoline tetramers are represented by the yellow and red areas, respectively. (d) Bilayer structure of **20** viewed along the *b* axis. Orange and blue areas indicate the D–π–A and alkyl chain layers, respectively. Hydrogen atoms are omitted in (c) and (d), and alkyl chains are omitted in (c).

3CNQ ring with $\theta_1 = 5.2°$ and $\theta_2 = 7.9°$ (Figure 15a). The alkyl chain bent at the first methylene carbon atom to avoid steric hindrance with the 3CNQ moiety, and extended parallel to the 3CNQ moiety (Figure 15b). In the crystal structure, the 3CNQ moiety and alkyl chain alternately stacked to form a one-dimensional columnar structure along the *a* axis (yellow areas in Figures 15c and 15d). Instead of the 3CNQ moiety, the indoline moiety formed a head-to-tail dimer with an interplanar distance of 3.42 Å (red areas in Figures 15c and 15d).

The alternating stacking structure of 3CNQ moieties and alkyl chains observed in this crystal was not seen for other $\mathbf{I}_n$–3CNQ crystals, since the 3CNQ moiety has a strong tendency to form a dimer unit or columnar structure. The similar lengths of the 3CNQ moiety and alkyl chain may give rise to this uncommon type of π-alkyl alternating stack structure (Figures 15a and 15b).

$\mathbf{I}_{20}$–3CNQ (20): Crystal **20** was obtained by recrystallization from hexane and crystallized in a triclinic system. There were two crystallographically independent molecules $\mathbf{20^I}$ and $\mathbf{20^{II}}$. Both $\mathbf{20^I}$ and $\mathbf{20^{II}}$ molecules had a Type II conformation with $\theta_3 = 158.0$ and 165.2°, respectively (Figures 16a and 16b). In both molecules, the alkyl groups extended nearly perpendicular to the molecular long axis and parallel to the molecular plane. 3CNQ moieties stacked to form a tetramer unit in the sequence $\mathbf{20^{II}}$–$\mathbf{20^I}$–$\mathbf{20^I}$–$\mathbf{20^{II}}$ (yellow areas in Figure 16c). The face-to-face distances were 3.41 Å for the $\mathbf{20^I}$–$\mathbf{20^I}$ and ca. 3.6 Å for the $\mathbf{20^I}$–$\mathbf{20^{II}}$ stacks where the dihedral angle between the two 3CNQ moieties was 14.9°. An inversion center was located at the center of the $\mathbf{20^I}$–$\mathbf{20^I}$ stack. In addition to the 3CNQ stacks, π-stacks of indoline moieties formed a $\mathbf{20^I}$–$\mathbf{20^{II}}$–$\mathbf{20^{II}}$–$\mathbf{20^I}$ tetramer (red area in Figure 16c). The face-to-face distances were 3.79 Å for the $\mathbf{20^{II}}$–$\mathbf{20^{II}}$ and ca. 3.7 Å for the $\mathbf{20^I}$–$\mathbf{20^{II}}$ stacks, where the dihedral angle between the two indoline moieties was 6.3°. An inversion center was located at the center of the $\mathbf{20^{II}}$–$\mathbf{20^{II}}$ stack. These face-to-face interactions formed a D–π–A ribbon structure parallel to the *a* axis (Figure 16c). In addition, the self-aggregation of long alkyl chains formed a two-dimensional sheet structure parallel to the *ab* plane (blue area in Figure 16d). This crystal was constructed by alternation of the D–π–A and alkyl chain layers.

Self-aggregation ability of π-moieties and alkyl chains sim-

ilar to that of **20** has been observed in TTC_n-TTF molecules having long alkyl chains[19a] and also in the C_7TET-TTF·TCNQ complex[19b] (C_7TET-TTF = bis(heptylthio)ethylenedithio-TTF, Chart 1), where strong interchain interactions assist a proximate face-to-face contact of π-moieties (Fastener effect). In particular, the bilayer structure composed of a π-layer and alkyl-layer observed in **20** is reminiscent of that of the C_7TET-TTF·TCNQ complex. This result clearly indicates that the self-aggregation of alkyl chains is dominant in this crystal.

Structural Parameters Relating to Molecular and Electronic Structures of I_n–3CNQ. (A) Molecular Conformations, Type I vs. Type II: Among I_n–3CNQ-R molecules with short alkyl groups ($n = 1$), I_1–3CNQ-F_4 (**A**), (I_1–3CNQ-F_2)$(MeCN)_{0.5}$ (**C**), (I_1–3CNQ-F_1)$(MeCN)_{0.5}$ (**Db**), I_1–3CNQ-F_1 (**Dc**), I_1–3CNQ-$(MeO)_2$ (**E**), (I_1–3CNQ-$(EtO)_2$)(MeCN) (**Fa**), and I_1–3CNQ-$(EtO)_2$ (**Fb**) have a Type I conformation, and (I_6–3CNQ-CF_3) (**B**) and I_1–3CNQ-F_1 (**Da**) have a Type II conformation (Scheme 2).[25] For longer alkyl chain derivatives, only **3a** and **10** have molecules with a Type I conformation, while the remaining crystals have molecules with a Type II conformation.

As described above, Type I and II conformations for I_n–3CNQ would depend on the steric repulsion between the *N*-alkyl chain and the CN1 group also in the solid state, and short and long alkyl chain derivatives favor Type I and II, respectively. Demonstrating this hypothesis, I_1–3CNQ-R[25] and I_3–3CNQ (**3a** and **3b**) produced molecules of both Type I and II conformations depending on the crystallization conditions. While I_6–3CNQ showed only Type II conformation irrespective of the recrystallization conditions (solvents hexane/benzene for **6a** and **6b**, and MeCN for **6c**), and the substituted I_6–3CNQ-R ($R = CF_3$)[25] molecule also have only Type II conformation in the crystal structures. Furthermore, in the crystal structures of analogous **D**–3CNQ compounds having D moieties, which do not possess bulky groups on the site opposite to the *N*-alkyl chain (3,3-dimethyl group in the case of I_n–3CNQ), molecules have only the Type II conformation.[10,11,26]

The most important feature of the molecular conformation of I_n–3CNQ is the difference in the degree of CT (δ) between the Type I and II conformations, where molecules with Type I conformation (**3a** and **10**) possessed larger δ values than those with Type II conformation, which will be discussed later.

(B) π-Stacking of D–π–A Skeleton and Self-Aggregation of Alkyl Chain: The most important factor in the crystal structures of I_n–3CNQ derivatives is the dimerization of 3CNQ moieties to cancel the large molecular dipole moment. Dimerized motifs of 3CNQ moieties were observed in most of the crystals in this study and also in the crystal structures of I_n–3CNQ-R derivatives **A**–**F**[25] and other **D**–3CNQ compounds.[10,11,26] Due to the formation of centrosymmetric π-stacking motifs, second-order non-linear optical properties such as second harmonic generation are not expected for bulk I_n–3CNQ crystals, and alignment of the dipole moments to form non-centrosymmetric systems is necessary. While π-stacking motifs of **2**, **3b**, and **10** preserved the non-centrosymmetric structures, π-stacks on indoline moieties and/or side-by-side dimerization cancelled the dipole moments of bulk crystals. Although several I_n–3CNQ compounds formed segregated π-stacking structures of the indoline and/or 3CNQ moieties, they were insulators (room temperature conductivity $<10^{-8}$ S cm^{-1}).

With increasing alkyl chain lengths ($n \geq 6$), the self-assembling ability of alkyl chains was activated. The balance between dimerization of the 3CNQ moieties and the self-assembling ability of alkyl chains depended on *n* and constructed diverse molecular packings. In the I_n–3CNQ crystals ($n = 6$–8), the alkyl chains formed aggregated structures parallel to the π-stacking structures of D–π–A skeletons (tetramer unit or one-dimensional column). In the case of I_{10}–3CNQ, similar lengths of the 3CNQ skeleton and alkyl chain resulted in a strong interaction, preventing face-to-face interaction of the D–π–A skeleton, and the formation of alternating stack of 3CNQ moieties and alkyl chains. For the further longer alkyl chain I_n–3CNQ, self-aggregation of alkyl chains became dominant resulting in the formation of the bilayer structure of **20** formed by alkyl chain layers and D–π–A layers.

(C) Bond Length Ratio (*BLR*) vs. Intramolecular Degree of CT (δ): Bond alternation of the I_n–3CNQ molecule is represented by the mixing of two resonance structures of neutral ($\delta = 0$) and ionic ($\delta = 1$) forms (Scheme 3). Therefore, intramolecular bond lengths are expected to be sensitive to the δ value. Such bond length alternation, which relates to two res-

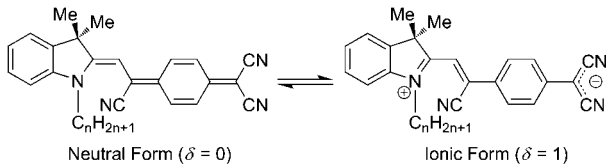

Scheme 3. Resonance structures of I_n–3CNQ in neutral ($\delta = 0$) and ionic ($\delta = 1$) forms.

Table 3. Selected Intramolecular Bond Lengths (Å[a]) of I_n–3CNQ Molecules

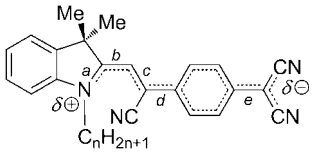

		a/Å	*b*/Å	*c*/Å	*d*/Å	*e*/Å
I_2–3CNQ	**2**	1.348(3)	1.407(3)	1.376(3)	1.440(3)	1.410(3)
I_3–3CNQ	**3a**	1.326(2)	1.429(2)	1.373(2)	1.443(2)	1.428(2)
	3b	1.346(2)	1.411(2)	1.391(2)	1.438(2)	1.421(2)
I_4–3CNQ	**4**	1.357(4)	1.400(5)	1.387(5)	1.436(4)	1.409(5)
I_5–3CNQ	**5**	1.349(3)	1.401(3)	1.385(3)	1.432(3)	1.410(3)
I_6–3CNQ	**6a**	1.347(3)	1.397(3)	1.398(3)	1.427(3)	1.408(3)
	6b	1.355(4)	1.389(4)	1.394(4)	1.431(4)	1.407(5)
	6c	1.351(3)	1.403(3)	1.388(3)	1.435(3)	1.417(3)
I_7–3CNQ	**7a^{I}**	1.354(6)	1.398(7)	1.401(7)	1.420(7)	1.414(7)
	7a^{II}	1.350(6)	1.395(7)	1.392(7)	1.431(7)	1.407(7)
	7b	1.355(4)	1.399(4)	1.392(4)	1.428(4)	1.410(4)
I_8–3CNQ	**8^{I}**	1.356(2)	1.394(2)	1.395(2)	1.427(2)	1.406(2)
	8^{II}	1.354(2)	1.396(2)	1.396(2)	1.420(2)	1.401(3)
I_{10}–3CNQ	**10**	1.328(2)	1.421(2)	1.374(2)	1.441(2)	1.423(2)
I_{20}–3CNQ	**20^{I}**	1.355(5)	1.392(6)	1.388(6)	1.426(6)	1.417(7)
	20^{II}	1.338(6)	1.383(7)	1.386(7)	1.419(7)	1.397(7)

a) 1 Å = 0.1 nm.

Table 4. Bond Length Ratio (*BLR*), Estimated Degree of CT from *BLR* (δ_{BLR}), Dipole Moments in Ground and Excited States (μ_g and μ_e, Respectively), and Estimated Degrees of CT from Atomic Charge and Dipole Moments (δ_{charge} and δ_{dipole}, Respectively) of Type I and II $\mathbf{I}_n$–3CNQ-R Molecules

Symbol	Molecule	*BLR*	δ_{BLR}	δ_{charge}[a)]	μ_g/Debye[a)]	μ_e/Debye[a)]	δ_{dipole}	Reference
Type I								
A	$\mathbf{I}_1$–3CNQ-F_4	1.624(3)	0.93	0.66	27.1	10.2	0.73	25
C	$\mathbf{I}_1$–3CNQ-F_2	1.615(3)	0.90	0.64	25.9	10.8	0.71	25
Db	$\mathbf{I}_1$–3CNQ-F_1b[b)]	1.599(3)	0.83	0.61	23.8	10.5	0.69	25
Dc		1.611(5)	0.88	0.66	25.5	8.4	0.75	25
3a	$\mathbf{I}_3$–3CNQ	1.593(2)	0.80	0.55	22.6	13.1	0.63	this work
10	$\mathbf{I}_{10}$–3CNQ	1.586(2)	0.77	0.55	21.9	12.7	0.63	this work
E[c)]	$\mathbf{I}_1$–3CNQ-$(MeO)_2$	1.530(2)	0.52	0.39	15.9	15.7	0.50	25
Fa	$\mathbf{I}_1$–3CNQ-$(EtO)_2$	1.531(8)	0.53	0.42	17.1	15.2	0.53	25
Fb	$\mathbf{I}_1$–3CNQ-$(EtO)_2$	1.526(7)	0.51	0.37	15.5	16.0	0.49	25
Type II								
B	$\mathbf{I}_6$–3CNQ-CF_3	1.566(4)	0.68	0.43	20.0	17.9	0.53	25
Da^{I}[c)]	$\mathbf{I}_1$–3CNQ-3-F_1a[b)]	1.583(4)	0.76	0.40	18.7	15.1	0.55	25
Da^{II}[c)]		1.556(4)	0.64	0.43	16.8	15.7	0.52	25
2	$\mathbf{I}_2$–3CNQ	1.563(3)	0.67	0.41	17.1	15.1	0.53	this work
3b	$\mathbf{I}_3$–3CNQ	1.560(2)	0.66	0.41	17.4	16.0	0.52	this work
4	$\mathbf{I}_4$–3CNQ	1.547(4)	0.60	0.39	16.5	15.6	0.51	this work
5	$\mathbf{I}_5$–3CNQ	1.552(3)	0.62	0.40	16.7	15.7	0.51	this work
6a	$\mathbf{I}_6$–3CNQ	1.542(3)	0.58	0.38	16.3	16.6	0.50	this work
6b		1.538(4)	0.56	0.37	16.2	16.5	0.49	this work
6c[d)]		1.553(3)	0.63	0.40	17.1	15.4	0.53	this work
7a^{I}	$\mathbf{I}_7$–3CNQ	1.536(7)	0.55	0.38	16.2	16.6	0.49	this work
7a^{II}		1.544(7)	0.59	0.38	16.3	16.4	0.50	this work
7b[d)]		1.542(4)	0.58	0.38	15.9	16.5	0.49	this work
8^{I}	$\mathbf{I}_8$–3CNQ	1.537(2)	0.55	0.38	15.3	15.8	0.49	this work
8^{II}		1.533(2)	0.54	0.37	15.2	16.4	0.48	this work
20^{I}	$\mathbf{I}_{20}$–3CNQ	1.544(6)	0.59	0.38	15.9	16.5	0.49	this work
20^{II}		1.541(7)	0.57	0.39	15.7	16.1	0.49	this work

a) Calculated with the INDO/S parameterization using structures extracted from crystal structures. b) $\mathbf{I}_1$–3CNQ-F_1a and $\mathbf{I}_1$–3CNQ-F_1b are the isomers relating to the substituent positions on the 3CNQ moiety, where F atoms are connected at 2- or 6-, and 3- or 5-positions of the benzenoid ring, respectively. c) Orientation disorder of the substituent groups on the 3CNQ moiety was observed for **Da** and **E**. Molecular orbital (MO) calculations were performed using structures with larger occupancies. d) Orientation disorder of the alkyl chain was observed for **6c** and **7b**, and MO calculations were performed using structures with idealized alkyl chains instead of disordered ones.

onance structures in an organic polymethine dye, has been utilized for the evaluation of molecular (hyper)polarizabilities.[27–29] In intermolecular CT solids, a good linear relationship between the degree of intermolecular CT, an essential parameter governing electronic properties and phase transitions, and bond lengths was observed in TCNQ[30] and BEDT-TTF (bis(ethylenedithio)-TTF, Chart 1) systems,[31] which are the components of organic metals and (super)conductors.[32] Similar to these systems, bond length analysis would provide crucial experimental information on the δ value of the $D^{\delta+}$–π–$A^{\delta-}$ molecules and would provide a methodology to analyze and understand their physical properties.

In the bond alternation of the $\mathbf{I}_n$–3CNQ-R system between neutral ($\delta = 0$) and ionic ($\delta = 1$) forms, bonds ***a*** and ***c*** have a single- or double-bond character, and bonds ***b***, ***d***, and ***e*** have a double- or single-bond character, respectively (Scheme 3 and Table 3). Table 3 summarizes the bond lengths ***a***–***e*** in the crystal structures of **2**–**8**, **10**, and **20**. Here, we have defined the bond length ratio (*BLR*), $(\boldsymbol{b} + \boldsymbol{d} + \boldsymbol{e})/(\boldsymbol{a} + \boldsymbol{c})$, as an index of δ in the $\mathbf{I}_n$–3CNQ system. *BLR* values for $\delta = 0$ and 1 limits were calculated as 1.410 and 1.639, respectively, by applying the single and double bond lengths of C–N bonds in an indoline moiety (1.384 and 1.324 Å, respectively)[33] for ***a***, and of C–C bonds in a π-conjugated $-(C{=}C{-}C)_x-$ chain (1.451 and 1.332 Å, respectively)[34] for ***b***–***e***. The δ values from *BLR* (δ_{BLR}) were obtained by eq 5 assuming a linear relationship of δ_{BLR} and *BLR*. The results are summarized in Table 4, where the data for $\mathbf{I}_n$–3CNQ-R (R = F_4, F_2, CF_3, F_1, $(MeO)_2$, and $(EtO)_2$) molecules are also tabulated for the following discussion concerning δ.[25]

$$\delta_{BLR} = 4.37 \cdot BLR - 6.16 \quad (5)$$

Since the $\delta_{BLR} = 0$ and 1 limits for the $\mathbf{I}_n$–3CNQ-R system have not been determined, we could not calculate distinct δ values from *BLR* analysis; therefore, the following discussion is limited to only qualitative values. We will discuss the relationships between *BLR* or δ_{BLR} values and those estimated by other methods and related parameters.

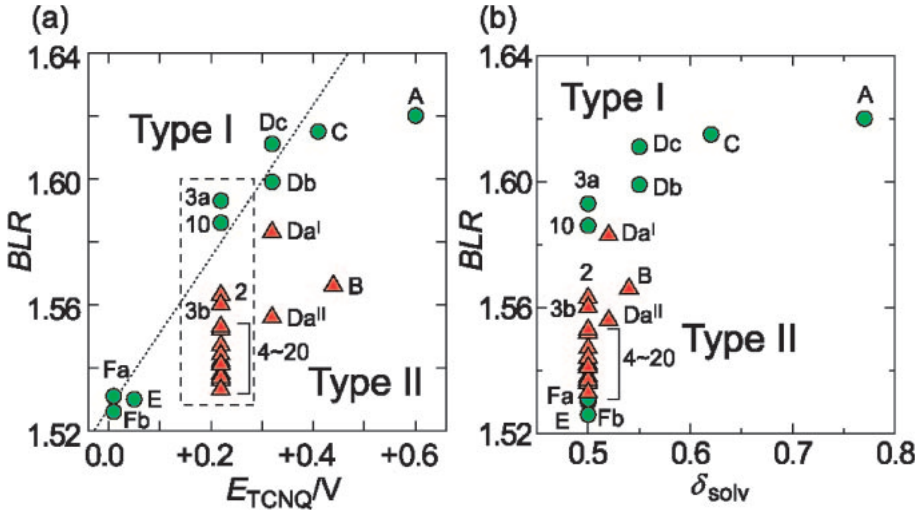

Figure 17. Plot of (a) *BLR* vs. E_{TCNQ} and (b) *BLR* vs. δ_{solv} for $\mathbf{I}_n$–3CNQ-R molecules.[25] The green circles and red triangles indicate molecules of Type I and II conformations, respectively, and the numbers and symbols correspond to those in Table 4. $E_{TCNQ} = +0.60$ (F_4), $+0.44$ (CF_3), $+0.41$ (F_2), $+0.32$ (F_1), $+0.22$ (H), $+0.05$ ($(MeO)_2$), and $+0.01$ ($(EtO)_2$) V vs. SCE. $\delta_{solv} = 0.77$ (**A**), 0.54 (**B**), 0.62 (**C**), 0.52 (**Da**), 0.55 (**Db** and **Dc**), 0.50 (**E**), and 0.50 (**Fa** and **Fb**). The dotted line and rectangle in (a) indicate the least-squares fits for molecules of Type I conformation except for **A** and the plots of $\mathbf{I}_n$–3CNQ (R = H) molecules, respectively.

(D) Relationship between *BLR* and Acceptor Strength of 3CNQ Part or Molecular Conformation: Figure 17a shows a plot of the *BLR* values of $\mathbf{I}_n$–3CNQ-R vs. the acceptor strength of each 3CNQ-R part evaluated by the first reduction potential of corresponding R-TCNQ derivative (E_{TCNQ}) in the CV measurement. Although the plot had a large scatter, *BLR* values (also δ_{BLR}) increased with increase in E_{TCNQ}, indicating that these *BLR* values roughly represent δ of the $\mathbf{I}_n$–3CNQ-R molecules. It is noteworthy that there is a considerable difference between *BLR* values for molecules of Type I and II conformation: the molecules of Type I conformation (**3a** and **10**) had larger *BLR* values (1.593 and 1.586, respectively) than those of Type II (1.533–1.563) as shown in the dotted rectangle in Figure 17a, indicating a larger degree of CT of molecules of Type I conformation. As discussed above, this result can probably be attributed to the Coulombic interaction between the negatively charged CN1 group and the indoline moiety. The larger *BLR* values of molecules of Type I conformation which is more favorable for smaller *n* derivatives coincide with the result of solvatochromism.

Furthermore, in a sharp contrast to the small effect of the alkyl chain length ($n \geq 2$) on the solution properties (redox properties and solvatochromism), Type II $\mathbf{I}_n$–3CNQ molecules had a wide range of *BLR* (1.533–1.563) and δ_{BLR} (0.54–0.67) values and showed a strong dependency on alkyl chain length in the crystals (Table 4 and Figure 17b). These results indicate that not only molecular geometry (i.e. conformation and planarity) but also crystal packing has a significant effect on δ in the solid state.

(E) Degree of CT and Molecular Packing: Figure 18 plots the *BLR* value of $\mathbf{I}_n$–3CNQ molecule against alkyl chain length (*n*), where very similar tendency to that of melting points against *n* (Figure 1) was presented. In the range of $n = 2$–8, *BLR* values of Type II molecules decreased with the increment of *n*. A systematic relationship was not found between *BLR* and molecular arrangements (alternating or segregated columns, and isolated dimers or tetramers). The dependence of *BLR* values on *n* probably originates from the density of D–π–A skeleton in the crystal; the higher one causes the highly polar crystalline field in a bulk crystal to afford the larger *BLR* (δ) value. Elongation of the alkyl chain decreases the density of D–π–A skeleton as well as the *BLR* value. While, the *BLR* values of $\mathbf{I}_{20}$–3CNQ are larger than or close to those of $n = 6$–8 compounds. It is plausible that the strong self-aggregation ability of long alkyl chains as shown in Figure 16d formed a tight molecular packing of the D–π–A skeleton,

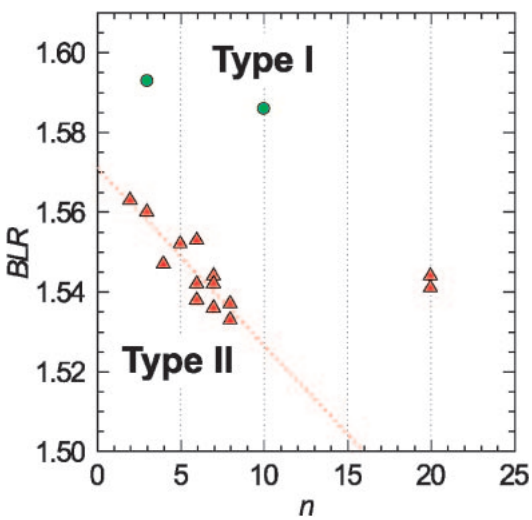

Figure 18. Plot of *BLR* vs. alkyl chain length (*n*) for $\mathbf{I}_n$–3CNQ molecules. Green circles and red triangles indicate molecules of Type I and II conformations, respectively. The dotted line indicates the least-squares fit for molecules of Type II conformation ($n = 2$–8).

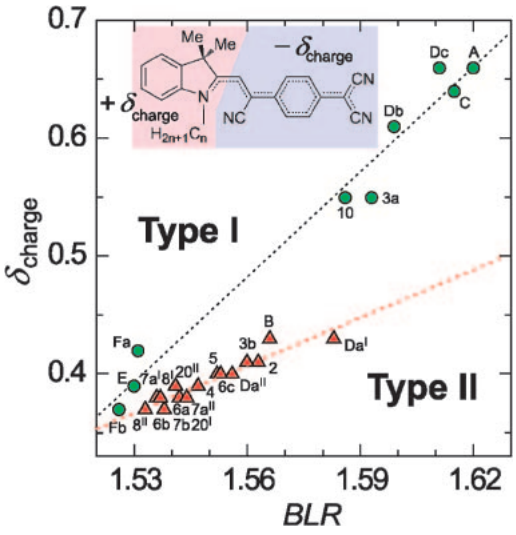

Figure 19. Plot of δ_{charge} vs. *BLR* for $\mathbf{I}_n$–3CNQ-R molecules. Green circles and red triangles indicate molecules of Type I and II conformations, respectively. The lines represent least-squares fits for each plot. The numbers and symbols in the figure correspond to those in Table 4. The chemical structure indicates the separation of D (red) and A (blue) moieties. In this study, the π-bridge is included in the A moiety because it has a negative charge.

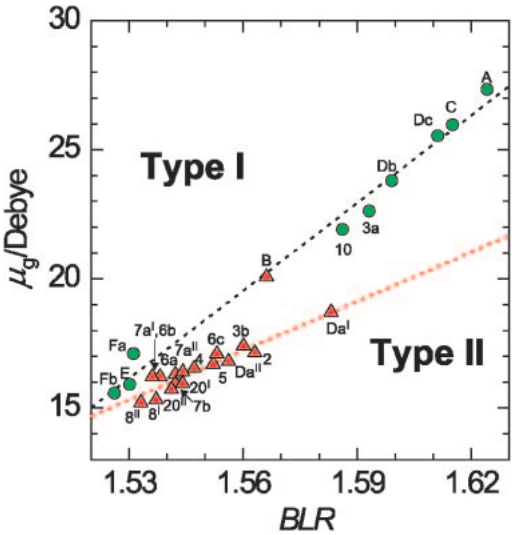

Figure 20. Plot of the ground state dipole moment (μ_g) of $\mathbf{I}_n$–3CNQ-R by the INDO/S MO calculation against *BLR*. Green circles and red triangles represent molecules of Type I and II conformations, respectively. The lines in each plot represent the least-squares fits to the data excepting **B**, and the numbers and symbols correspond to those in Table 4.

resulting in the large *BLR* (δ) values.

(F) Calculated Degrees of CT and Dipole Moments: The *BLR* value is inadequate to quantitatively estimate the spatial charge distribution of an $\mathbf{I}_n$–3CNQ molecule, because the $\delta = 0$ and 1 limits of $\mathbf{I}_n$–3CNQ-R are unknown. To find a more appropriate expression of the δ value which also considers effects on *BLR*, we have examined molecular orbital (MO) calculations using structures extracted from the crystal structures, and investigated the relationship between *BLR* and δ values obtained from the atomic charge and dipole moments.

The degree of CT for atomic charge (δ_{charge}) was obtained from the sum of atomic charges of the D and A parts (Figure 19). The results are summarized in Table 4. Figure 19 plots the relationship between δ_{charge} and *BLR*: δ_{charge} increased linearly with *BLR* in agreement with the prediction made from the bond alternation and the relationship between E_{TCNQ} and *BLR*. Molecules of Type I and II conformation exhibited different linear relationships between δ_{charge} and *BLR*: molecules of Type I conformation possessed a greater slope than those of Type II. The calculated δ_{charge} values were lower by 0.13–0.46 than those of δ_{BLR} for all compounds probably because of the indefinite *BLR* values for the $\delta = 0$ and 1 limits, and the arbitrariness in the separation of the D and A moieties of the $\mathbf{I}_n$–3CNQ molecule.

In order to eliminate the ambiguities in the δ_{BLR} and δ_{charge} values, we have examined dipole moments (μ) obtained by MO calculation. Figure 20 plots the dipole moment of the $\mathbf{I}_n$–3CNQ-R molecule in the ground state (μ_g, Table 4) against *BLR* value. Similar to the δ_{charge}, the μ_g value increased with *BLR*, and molecules of Type I and II conformations showed two kinds of linear relationships: only **B** of Type II deviated from the plot. Here, we estimated the degree of CT using calculated dipole moments (δ_{dipole}).

In general, the dipole moments of the ground (μ_g) and excited (μ_e) states of a $D^{\delta+}$–π–$A^{\delta-}$ molecule are approximately expressed as

$$\mu_g = \delta ed \tag{6}$$

$$\mu_e = (1 - \delta)ed \tag{7}$$

Here, e and d are the elementary electric charge and distance between averaged centers of positive and negative charges, respectively. The difference ($\mu_e - \mu_g$) and sum ($\mu_e + \mu_g$) of dipole moments are expressed as

$$\mu_e - \mu_g = (1 - 2\delta)ed \tag{8}$$

$$\mu_e + \mu_g = ed \tag{9}$$

Figures 21a and 21b compare μ_g, μ_e, dipole difference ($\mu_e - \mu_g$), and sum ($\mu_e + \mu_g$) for the $\mathbf{I}_n$–3CNQ-R molecules with Type I and II conformations, respectively. Plots of each parameter exhibited good linear relationships with *BLR*. The dipole difference ($\mu_e - \mu_g$) crossed the zero point, which, according to eq 8, should correspond to $\delta = 0.5$ at approximately $BLR = 1.53$ for Type I and 1.54 for Type II conformations. These values are similar to the *BLR* value (1.52) for $\delta_{BLR} = 0.5$, determined from eq 5. Assuming a simple linear relationship of δ and *BLR* in eq 5, the ($\mu_g + \mu_e$) value, which is a function of d (eq 9) and independent of δ, should be constant with respect to *BLR*. However, the ($\mu_g + \mu_e$) value steadily increases with *BLR* for the $\mathbf{I}_n$–3CNQ-R system, suggesting that the charge distance d varies with respect to the ionicity, position of substituents, molecular conformation, etc.

Here, we utilized a more appropriate parameter pertaining to the degree of CT while considering the relationship illustrated in Figures 21a and 21b. The intramolecular degree of CT

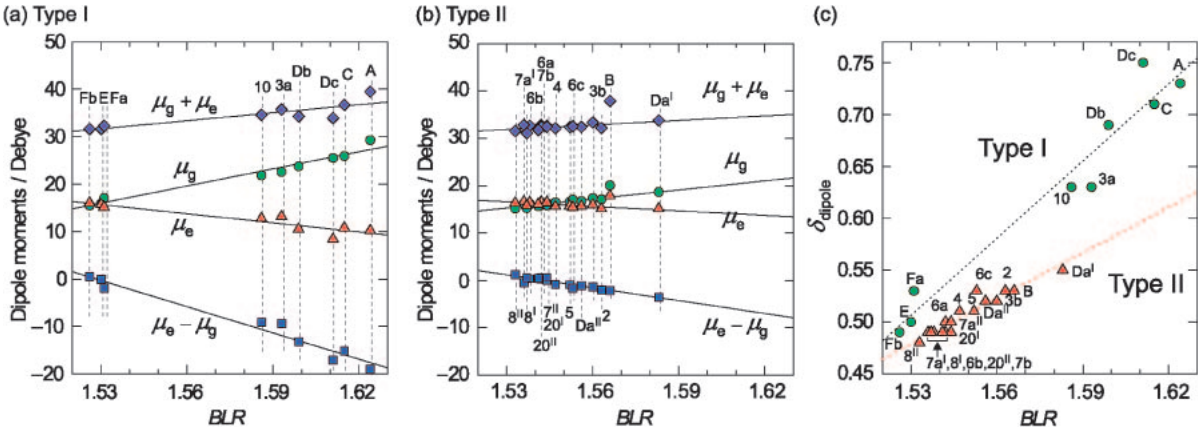

Figure 21. Plots of calculated dipole moments of the ground (μ_g, green circles) and excited (μ_e, red triangles) states, dipole difference ($\mu_e - \mu_g$, blue squares), and sum ($\mu_g + \mu_e$, purple diamonds) vs. *BLR* for the $\mathbf{I}_n$–3CNQ-R molecules with Type I (a) and Type II (b) conformations. (c) Plot of *BLR* vs. δ_{dipole} for $\mathbf{I}_n$–3CNQ-R. The green circles and red triangles represent molecules of Type I and II conformations, respectively. The lines in each plot represent the least-squares fits to the data.

based on the dipole moment (δ_{dipole}), which is derived from eqs 6 and 9 and does not include the uncertain d value, is expressed as

$$\mu_g/(\mu_e + \mu_g) = \delta_{dipole} \quad (10)$$

The δ_{dipole} values reproduce the calculated dipole moments, and hence, reflect the effects of molecular conformation, position of substituent groups, and change in d. The calculated δ_{dipole} values were smaller than δ_{BLR} but larger than δ_{charge} for all compounds (Table 4). Figure 21c plots the calculated δ_{dipole} vs. *BLR*. Similar to δ_{charge} and μ_g, the δ_{dipole} values exhibited a good linear relationship with *BLR*. Molecules of Type I conformation had larger δ_{dipole} values and greater slope than those of Type II conformation. The δ_{dipole} values also contain some ambiguities because of the difference in charge distances in the ground and excited states; however, it should be emphasized that the *BLR* values of the $\mathbf{I}_n$–3CNQ-R molecules estimated from the crystal structures exhibited a good linear relationship with the δ values obtained from the MO calculation. This investigation undoubtedly confirms that the *BLR* reflects the δ values of D–π–A compounds and is a useful experimental parameter to investigate their functionalities.

Conclusion

A series of intramolecular CT compounds, indoline–tricyanoquinodimethane ($\mathbf{I}_n$–3CNQ) derivatives with alkyl chains of various lengths (n = 1–8, 10, 14, 16, 18, 20, and 22) were prepared and structurally characterized. The melting points of $\mathbf{I}_n$–3CNQ steadily decreased with increase in alkyl chain length up to the minimum point of 95 °C (n = 18), and the compounds with $n \geq 6$ formed a supercooled liquid after melting. In the crystal structures, diverse molecular arrangements were observed based on the alkyl chain length among which the dimerization of 3CNQ moieties was the most common. The self-assembling ability of alkyl chains became more active with increasing alkyl chain length ($n \geq 6$) to construct one-dimensional segregated structures or two-dimensional bilayer structures of D–π–A and alkyl chain moieties. We proposed a new structural parameter, bond length ratio (*BLR*), for the $\mathbf{I}_n$–3CNQ-R system as an indicator of the degree of intramolecular CT (δ) in the crystal structures. The comparison of *BLR* with δ values estimated from the MO calculations (δ_{charge} and δ_{dipole}) confirmed that *BLR* is a suitable parameter to qualitatively express δ value of a $D^{\delta+}$–π–$A^{\delta-}$ compound, although the definite δ value could not be obtained. The balance of steric repulsion between the *N*-alkyl chain and the neighboring CN group produced two types of molecular conformations, namely Type I and II, in which the *N*-alkyl group locates close to and far from the CN1 group, respectively. The conformation depended on the alkyl chain length in both solution and solid states, and Type II conformation was preferred for long alkyl chain molecules. Our analyses also revealed that the δ value is determined not only by the substituent effect on the 3CNQ moiety but also by the molecular conformation; the Type I conformation has a larger δ value than that of Type II. Furthermore, the self-aggregation ability of long alkyl chain compound (n = 20) formed a tight molecular packing of D–π–A skeleton causing the increment of the δ values. We emphasize that our investigation proposed methodologies to elucidate and control the electronic structure of a $D^{\delta+}$–π–$A^{\delta-}$ compound in the solid state, and disclosed the importance of molecular conformation and molecular packing. These studies will provide a new strategy in the molecular design of $D^{\delta+}$–π–$A^{\delta-}$ compounds and will contribute to the development of organic functional materials based on these molecular systems.[1–12,20,27–29]

This work was partly supported by a Grant-in-Aid (21st Century COE programs on Kyoto University Alliance for Chemistry and No. 15205019) from the Ministry of Education, Culture, Sports, Science and Technology, Japan. T. M. is a recipient of a Japan Society for the Promotion of Science (JSPS) research fellowship.

Supporting Information

Selected physical data, UV–vis, DSC measurements, crystallographic data, and cyclic voltammograms for $\mathbf{I}_n$–3CNQ. This material is available free of charge at http://www.csj.jp/journals/bcsj/.

References

1 R. M. Metzger, B. Chen, U. Höpfner, M. V. Lakshmikantham, D. Vuillaume, T. Kawai, X. Wu, H. Tachibana, T. V. Hughes, H. Sakurai, J. W. Baldwin, C. Hosch, M. P. Cava, L. Brehmer, G. J. Ashwell, *J. Am. Chem. Soc.* **1997**, *119*, 10455.

2 J. W. Baldwin, B. Chen, S. C. Street, V. V. Konovalov, H. Sakurai, T. V. Hughes, C. S. Simpson, M. V. Lakshmikantham, M. P. Cava, L. D. Kispert, R. M. Metzger, *J. Phys. Chem. B* **1999**, *103*, 4269.

3 a) R. M. Metzger, *Acc. Chem. Res.* **1999**, *32*, 950. b) R. M. Metzger, *Chem. Rev.* **2003**, *103*, 3803. c) A. Honciuc, A. Otsuka, Y.-H. Wang, S. K. McElwee, S. A. Woski, G. Saito, R. M. Metzger, *J. Phys. Chem. B* **2006**, *110*, 15085. d) R. M. Metzger, *Anal. Chim. Acta* **2006**, *568*, 146.

4 a) G. J. Ashwell, R. Hamilton, L. R. H. High, *J. Mater. Chem.* **2003**, *13*, 1501. b) G. J. Ashwell, W. D. Tyrrell, A. J. Whittam, *J. Mater. Chem.* **2003**, *13*, 2855. c) G. J. Ashwell, A. Chwialkowska, L. R. H. High, *J. Mater. Chem.* **2004**, *14*, 2389. d) G. J. Ashwell, A. Chwialkowska, L. R. H. High, *J. Mater. Chem.* **2004**, *14*, 2848.

5 M. Szablewski, P. R. Thomas, A. Thornton, D. Bloor, G. H. Cross, J. M. Cole, J. A. K. Howard, M. Malagoli, F. Meyers, J.-L. Brédas, W. Wenseleers, E. Goovaerts, *J. Am. Chem. Soc.* **1997**, *119*, 3144.

6 G. J. Ashwell, *Thin Solid Films* **1990**, *186*, 155.

7 G. J. Ashwell, E. J. C. Dawnay, A. P. Kuczynski, M. Szablewski, I. M. Sandy, M. R. Bryce, A. M. Grainger, M. Hasan, *J. Chem. Soc., Faraday Trans.* **1990**, *86*, 1117.

8 H. E. Katz, K. D. Singer, J. E. Sohn, C. W. Dirk, L. A. King, H. M. Gordon, *J. Am. Chem. Soc.* **1987**, *109*, 6561.

9 M. Szablewski, *J. Org. Chem.* **1994**, *59*, 954.

10 a) N. A. Bell, D. J. Crouch, D. J. Simmonds, A. E. Goeta, T. Gelbrich, M. B. Hursthouse, *J. Mater. Chem.* **2002**, *12*, 1274. b) N. A. Bell, C. S. Bradley, R. A. Broughton, S. J. Coles, D. E. Hibbs, M. B. Hursthouse, A. K. Ray, D. J. Simmonds, S. C. Thorpe, *J. Mater. Chem.* **2005**, *15*, 1437.

11 a) R. M. Metzger, N. E. Heimer, G. J. Ashwell, *Mol. Cryst. Liq. Cryst.* **1984**, *107*, 133. b) G. J. Ashwell, J. R. Sambles, A. S. Martin, W. G. Parker, M. Szablewski, *J. Chem. Soc., Chem. Commun.* **1990**, 1374. c) A. S. Martin, J. R. Sambles, G. J. Ashwell, *Phys. Rev. Lett.* **1993**, *70*, 218.

12 A. M. Asiri, *Kuwait J. Sci. Eng.* **2003**, *30*, 71.

13 B. C. McKusick, R. E. Heckert, T. L. Cairns, D. D. Coffman, H. F. Mower, *J. Am. Chem. Soc.* **1958**, *80*, 2806.

14 D. Buckley, S. Dunstan, H. B. Henbest, *J. Chem. Soc.* **1957**, 4880.

15 A. Broo, M. C. Zerner, *Chem. Phys.* **1995**, *196*, 407.

16 M. Pickholz, M. C. dos Santos, *THEOCHEM* **1998**, *432*, 89.

17 C.-H. Chong, M. Makihara, G. Saito, *Mol. Cryst. Liq. Cryst.* **2002**, *376*, 183.

18 G. Saito, C.-H. Chong, M. Makihara, A. Otsuka, H. Yamochi, *J. Am. Chem. Soc.* **2003**, *125*, 1134.

19 a) Z. Shi, K. Imaeda, C. Nakano, H. Inokuchi, T. Enoki, G. Saito, *Mol. Cryst. Liq. Cryst.* **1995**, *268*, 161. b) A. Otsuka, G. Saito, T. Nakamura, M. Matsumoto, Y. Kawabata, K. Honda, M. Goto, M. Kurahashi, *Synth. Met.* **1988**, *27*, 575. c) P. Wu, G. Saito, K. Imaeda, Z. Shi, T. Mori, T. Enoki, H. Inokuchi, *Chem. Lett.* **1986**, 441. d) H. Yamochi, N. Iwasawa, H. Urayama, G. Saito, *Chem. Lett.* **1987**, 2265. e) N. Okada, H. Yamochi, F. Shinozaki, K. Oshima, G. Saito, *Chem. Lett.* **1986**, 1861.

20 Y. Ogata, J. Kawamata, C.-H. Chong, A. Yamagishi, G. Saito, *Clays Clay Miner.* **2003**, *51*, 181.

21 G. M. Sheldrick, *Program for the Solution of Crystal Structuers*, University of Göttingen, Göttingen, Germany, **1997**.

22 G. M. Sheldrick, *Program for the Refinement of Crystal Structures*, University of Göttingen, Göttingen, Germany, **1997**.

23 R. Foster, *Organic Charge-Transfer Complexes*, Academic Press, New York, **1969**.

24 C. Reichardt, *Chem. Rev.* **1994**, *94*, 2319.

25 Crystal structures of $\mathbf{I}_1$–3CNQ-R derivatives: T. Murata, G. Saito, K. Nishimura, C.-H. Chong, M. Makihara, G. Honda, Y. Enomoto, S. Khasanov, H. Yamochi, A. Otsuka, K. Kamada, K. Ohta, J. Kawamata, *Bull. Chem. Soc. Jpn.*, in press.

26 J. C. Cole, J. A. K. Howard, G. H. Cross, M. Szablewski, *Acta Crystallogr., Sect. C* **1995**, *51*, 715.

27 a) S. R. Marder, C. B. Gorman, B. G. Tiemann, J. W. Perry, G. Bourhill, K. Mansour, *Science* **1993**, *261*, 186. b) S. R. Marder, C. B. Gorman, F. Meyers, J. W. Perry, G. Bourhill, J.-L. Brédas, B. M. Pierce, *Science* **1994**, *265*, 632.

28 M. Barzoukas, C. Runser, A. Fort, M. Blanchard-Desce, *Chem. Phys. Lett.* **1996**, *257*, 531.

29 a) T. Kogej, D. Beljonne, F. Meyers, J. W. Perry, S. R. Marder, J. L. Brédas, *Chem. Phys. Lett.* **1998**, *298*, 1. b) D. Beljonne, T. Kogej, S. R. Marder, J. W. Perry, J. L. Brédas, *Nonlinear Opt.* **1999**, *21*, 461.

30 P. S. Flandrois, D. Chasseau, *Acta Crystallogr., Sect. B* **1977**, *33*, 2744.

31 P. Guionneau, C. J. Kepert, G. Bravic, D. Chasseau, M. R. Truter, M. Kurmoo, P. Day, *Synth. Met.* **1997**, *86*, 1973.

32 T. Ishiguro, K. Yamaji, G. Saito, *Organic Superconductors*, 2nd ed., Springer, Berlin, **1998**.

33 For ionic C–N bonds, we adopted the average value of seven crystal structures containing open-form spiropyrans (CCDC references: BAPNAH, BETGAI, GETGEM, FAFPOR, GUWFEJ, MOVYEB, and WOGKIM). For neutral C–N bonds, we adopted the average value of six crystals of indole-containing adducts (CCDC references: EADIND, EBASEF, GIYKOO, HMAJIO, XATFAZ, and ZIRFOV).

34 R. H. Baughman, B. E. Kohler, I. J. Levy, C. Spangler, *Synth. Met.* **1985**, *11*, 37.